



Universiteit Gent
Faculteit Wetenschappen
Vakgroep Fysica en Sterrenkunde

² No title yet

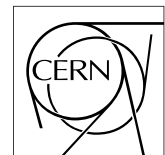
³ No sub-title neither, obviously...

⁴ Alexis Fagot

5



Thesis to obtain the degree of
Doctor of Philosophy in Physics
Academic years 2012-2017





Universiteit Gent
Faculteit Wetenschappen
Vakgroep Fysica en Sterrenkunde

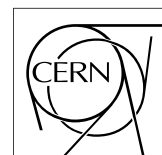
Promotoren: Dr. Michael Tytgat
Prof. Dr. Dirk Ryckbosch

Universiteit Gent
Faculteit Wetenschappen
Vakgroep Fysica en Sterrenkunde
Proeftuinstraat 86, B-9000 Gent, België
Tel.: +32 9 264.65.28
Fax.: +32 9 264.66.97

17



Thesis to obtain the degree of
Doctor of Philosophy in Physics
Academic years 2012-2017



Acknowledgements

¹⁹ Ici on remerciera tous les gens que j'ai pu croiser durant cette aventure et qui m'ont permis de passer
²⁰ un bon moment

²¹ *Gent, ici la super date de la mort qui tue de la fin d'écriture*
²² *Alexis Fagot*

Table of Contents

24	Acknowledgements	i
25	Nederlandse samenvatting	xv
26	English summary	xvii
27	1 Introduction	1-1
28	1.1 A story of High Energy Physics	1-1
29	1.2 Organisation of this study	1-1
30	2 Investigating the TeV scale	2-1
31	2.1 The Standard Model of Particle Physics	2-1
32	2.2 The Large Hadron Collider and the Compact Muon Solenoid	2-1
33	2.3 Muon Phase-II Upgrade	2-1
34	3 Amplification processes in gaseous detectors	3-1
35	3.1 Signal formation	3-1
36	3.2 Gas transport parameters	3-1
37	4 Resistive Plate Chambers	4-1
38	4.1 Principle	4-1
39	4.2 Rate capability of Resistive Plate Chambers	4-1
40	4.3 High time resolution	4-1
41	4.4 Resistive Plate Chambers at CMS	4-1
42	4.4.1 Overview	4-1
43	4.4.2 The present RPC system	4-2
44	4.4.3 Pulse processing of CMS RPCs	4-3
45	5 Longevity studies and Consolidation of the present CMS RPC subsystem	5-1
46	5.1 Testing detectors under extreme conditions	5-1
47	5.1.1 The Gamma Irradiation Facilities	5-3
48	5.1.1.1 GIF	5-3
49	5.1.1.2 GIF++	5-5
50	5.2 Preliminary tests at GIF	5-7
51	5.2.1 Resistive Plate Chamber test setup	5-7
52	5.2.2 Data Acquisition	5-9
53	5.2.3 Geometrical acceptance of the setup layout to cosmic muons	5-9
54	5.2.3.1 Description of the simulation layout	5-10
55	5.2.3.2 Simulation procedure	5-12
56	5.2.3.3 Results	5-13
57	5.2.4 Photon flux at GIF	5-13

58	5.2.4.1	Expectations from simulations	5-13
59	5.2.4.2	Dose measurements	5-18
60	5.2.5	Results and discussions	5-19
61	5.3	Longevity tests at GIF++	5-20
62	5.3.1	Description of the Data Acquisition	5-23
63	5.3.2	RPC current, environmental and operation parameter monitoring	5-24
64	5.3.3	Measurement procedure	5-25
65	5.3.4	Longevity studies results	5-25
66	6	Investigation on high rate RPCs	6-1
67	6.1	Rate limitations and ageing of RPCs	6-1
68	6.1.1	Low resistivity electrodes	6-1
69	6.1.2	Low noise front-end electronics	6-1
70	6.2	Construction of prototypes	6-1
71	6.3	Results and discussions	6-1
72	7	Conclusions and outlooks	7-1
73	7.1	Conclusions	7-1
74	7.2	Outlooks	7-1
75	A	A data acquisition software for CAEN VME TDCs	A-1
76	A.1	GIF++ DAQ file tree	A-1
77	A.2	Usage of the DAQ	A-2
78	A.3	Description of the readout setup	A-3
79	A.4	Data read-out	A-3
80	A.4.1	V1190A TDCs	A-4
81	A.4.2	DataReader	A-6
82	A.5	Communications	A-10
83	A.5.1	V1718 USB Bridge	A-10
84	A.5.2	Configuration file	A-11
85	A.5.3	WebDCS/DAQ intercommunication	A-14
86	A.5.4	Example of inter-process communication cycle	A-14
87	A.6	Software export	A-15
88	B	Details on the offline analysis package	B-1
89	B.1	GIF++ Offline Analysis file tree	B-1
90	B.2	Usage of the Offline Analysis	B-2
91	B.2.1	Output of the offline tool	B-3
92	B.2.1.1	ROOT file	B-3
93	B.2.1.2	CSV files	B-5
94	B.3	Analysis inputs	B-6
95	B.3.1	Dimensions file	B-6
96	C	Structure of the hybrid simulation software	C-1
97	C.1	Introduction	C-1

List of Figures

98

99	2.1	Absorbed dose in the CMS cavern after an integrated luminosity of 3000 fb. R is the transverse distance from the beamline and Z is the distance along the beamline from the Interaction Point at Z=0.	2-2
100			
101			
102	2.2	A quadrant of the muon system, showing DTs (yellow), RPCs (light blue), and CSCs (green). The locations of new forward muon detectors for Phase-II are contained within the dashed box and indicated in red for GEM stations (ME0, GE1/1, and GE2/1) and dark blue for improved RPC (iRPC) stations (RE3/1 and RE4/1).	2-2
103			
104			
105			
106	2.3	RMS of the multiple scattering displacement as a function of muon p_T for the proposed forward muon stations. All of the electromagnetic processes such as bremsstrahlung and magnetic field effect are included in the simulation.	2-3
107			
108			
109	4.1	Signals from the RPC strips are shaped by the FEE described on Figure 4.1a. Output LVDS signals are then read-out by a TDC module connected to a computer or converted into NIM and sent to scalers. Figure 4.1b describes how these converted signals are put in coincidence with the trigger.	4-3
110			
111			
112			
113	4.2	Description of the principle of a CFD. A comparison of threshold triggering (left) and constant fraction triggering (right) is shown in Figure 4.2a. Constant fraction triggering is obtained thanks to zero-crossing technique as explained in Figure 4.2b. The signal arriving at the input of the CFD is split into three components. A first one is delayed and connected to the inverting input of a first comparator. A second component is connected to the noninverting input of this first comparator. A third component is connected to the noninverting input of another comparator along with a threshold value connected to the inverting input. Finally, the output of both comparators is fed through an AND gate.	4-4
114			
115			
116			
117			
118			
119			
120			
121			
122	5.1	(5.1a) Extrapolation from 2016 data of single hit rate per unit area in the barrel region. (5.1b) Extrapolation from 2016 data of single hit rate per unit area in the endcap region.	5-2
123			
124			
125	5.2	Background Fluka simulation compared to 2016 Data at $L = 10^{34} \text{ cm}^{-2} \cdot \text{s}^{-1}$ in the fourth endcap disk region. A mismatch in between simulation and data can be observed. [To be understood.]	5-3
126			
127			
128	5.3	Layout of the test beam zone called X5c GIF at CERN. Photons from the radioactive source produce a sustained high rate of random hits over the whole area. The zone is surrounded by 8 m high and 80 cm thick concrete walls. Access is possible through three entry points. Two access doors for personnel and one large gate for material. A crane allows installation of heavy equipment in the area.	5-4
129			
130			
131			
132			
133	5.4	^{137}Cs decays by β^- emission to the ground state of ^{137}Ba (BR = 5.64%) and via the 662 keV isomeric level of ^{137}Ba (BR = 94.36%) whose half-life is 2.55 min.	5-5
134			

135	5.5	Floor plan of the GIF++ facility. When the facility downstream of the GIF++ takes electron beam, a beam pipe is installed along the beam line (z-axis). The irradiator can be displaced laterally (its center moves from $x = 0.65$ m to 2.15 m), to increase the distance to the beam pipe.	5-5
136			
137			
138			
139	5.6	Simulated unattenuated current of photons in the xz plane (Figure 5.6a) and yz plane (Figure 5.6b) through the source at $x = 0.65$ m and $y = 0$ m. With angular correction filters, the current of 662 keV photons is made uniform in xy planes.	5-6
140			
141			
142	5.7	Description of the RPC setup. Dimensions are given in mm. A tent containing RPCs is placed at 1720 mm from the source container. The source is situated in the center of the container. RE-4-2-BARC-161 chamber is 160 mm inside the tent. This way, the distance between the source and the chambers plan is 2060 mm. Figure 5.7a provides a side view of the setup in the xz plane while Figure 5.7b shows a top view in the yz plane.	5-7
143			
144			
145			
146			
147			
148	5.8	RE-4-2-BARC-161 chamber is inside the tent as described in Figure 5.7. In the top right, the two scintillators used as trigger can be seen. This trigger system has an inclination of 10° relative to horizontal and is placed above half-partition B2 of the RPCs. PMT electronics are shielded thanks to lead blocks placed in order to protect them without stopping photons from going through the scintillators and the chamber.	5-8
149			
150			
151			
152			
153	5.9	Hit distributions over all 3 partitions of RE-4-2-BARC-161 chamber is showed on these plots. Top, middle and bottom figures respectively correspond to partitions A, B, and C. These plots show that some events still occur in other half-partitions than B2, which corresponds to strips 49 to 64, in front of which the trigger is placed, contributing to the inefficiency of detection of cosmic muons. In the case of partitions A and C, the very low amount of data can be interpreted as noise. On the other hand, it is clear that a little portion of muons reach the half-partition B1, corresponding to strips 33 to 48.	5-9
154			
155			
156			
157			
158			
159			
160			
161	5.10	Results are derived from data taken on half-partition B2 only. On the 18 th of June 2014, data has been taken on chamber RE-2-BARC-161 at building 904 (Prevessin Site) with cosmic muons providing us a reference efficiency plateau of $(97.54 \pm 0.15)\%$ represented by a black curve. A similar measurement has been done at GIF on the 21 st of July with the same chamber giving a plateau of $(78.52 \pm 0.94)\%$ represented by a red curve.	5-10
162			
163			
164			
165			
166			
167	5.11	Representation of the layout used for the simulations of the test setup. The RPC is represented as a yellow trapezoid while the two scintillators as blue cuboids looking at the sky. A green plane corresponds to the muon generation plane within the simulation. Figure 5.7a shows a global view of the simulated setup. Figure 5.7b shows a zommed view that allows to see the 2 scintillators as well as the full RPC plane.	5-11
168			
169			
170			
171			
172	5.12	γ flux $F(D)$ is plot using values from table 5.1. As expected, the plot shows similar attenuation behaviours with increasing distance for each absorption factors.	5-14
173			
174	5.13	Figure 5.13a shows the linear approximation fit done via formulae 5.7 on data from table 5.2. Figure 5.13b shows a comparison of this model with the simulated flux using a and b given in figure 5.13a in formulae 5.4 and the reference value $D_0 = 50\text{cm}$ and the associated flux for each absorption factor F_0^{ABS} from table 5.1	5-16
175			
176			
177			
178	5.14	Dose measurements has been done in a plane corresponding to the tents front side. This plan is 1900 mm away from the source. As explained in the first chapter, a lens-shaped lead filter provides a uniform photon flux in the vertical plan orthogonal to the beam direction. If the second line of measured fluxes is not taken into account because of lower values due to experimental equipments in the way between the source and the tent, the uniformity of the flux is well showed by the results.	5-18
179			
180			
181			
182			
183			

184	5.15	5-19
185	5.16 Evolution of the maximum efficiency for RE2 (5.16a) and RE4 (5.16b) chambers	
186	with increasing extrapolated γ rate per unit area at working point. Both irradiated	
187	(blue) and non irradiated (red) chambers are shown.	5-21
188	5.17 Evolution of the working point for RE2 (5.17a) and RE4 (5.17b) with increasing	
189	extrapolated γ rate per unit area at working point. Both irradiated (blue) and non	
190	irradiated (red) chambers are shown.	5-21
191	5.18 Evolution of the maximum efficiency at HL-LHC conditions, i.e. a background hit	
192	rate per unit area of 300 Hz/cm ² , with increasing integrated charge for RE2 (5.18a)	
193	and RE4 (5.18b) detectors. Both irradiated (blue) and non irradiated (red) chambers	
194	are shown. The integrated charge for non irradiated detectors is recorded during test	
195	beam periods and stays small with respect to the charge accumulated in irradiated	
196	chambers.	5-22
197	5.19 Comparison of the efficiency sigmoid before (triangles) and after (circles) irradiation	
198	for RE2 (5.19a) and RE4 (5.19b) detectors. Both irradiated (blue) and non irradiated	
199	(red) chambers are shown.	5-22
200	5.20 Evolution of the Bakelite resistivity for RE2 (5.20a) and RE4 (5.20b) detectors. Both	
201	irradiated (blue) and non irradiated (red) chambers are shown.	5-23
202	5.21 Evolution of the noise rate per unit area for the irradiated chamber RE2-2-BARC-9	
203	only.	5-23
204	A.1 (A.1a) View of the front panel of a V1190A TDC module [10]. (A.1b) View of the	
205	front panel of a V1718 Bridge module [11]. (A.1c) View of the front panel of a 6U	
206	6021 VME crate [12].	A-3
207	A.2 Module V1190A <i>Trigger Matching Mode</i> timing diagram [10].	A-4
208	A.3 Structure of the ROOT output file generated by the DAQ. The 5 branches (<code>EventNumber</code> ,	
209	<code>number_of_hits</code> , <code>Quality_flag</code> , <code>TDC_channel</code> and <code>TDC_TimeStamp</code>) are visible on	
210	the left panel of the ROOT browser. On the right panel is visible the histogram cor-	
211	responding to the variable <code>nHits</code> . In this specific example, there were approximately	
212	50k events recorded to measure the gamma irradiation rate on the detectors. Each	
213	event is stored as a single entry in the <code>TTree</code>	A-10
214	A.4 WebDCS DAQ scan page. On this page, shifters need to choose the type of scan	
215	(Rate, Efficiency or Noise Reference scan), the gamma source configuration at the	
216	moment of data taking, the beam configuration, and the trigger mode. These in-	
217	formation will be stored in the DAQ ROOT output. Are also given the minimal	
218	measurement time and waiting time after ramping up of the detectors is over before	
219	starting the data acquisition. Then, the list of HV points to scan and the number of	
220	triggers for each run of the scan are given in the table underneath.	A-12

List of Tables

221

222 5.1	Total photon flux ($E\gamma \leq 662$ keV) with statistical error predicted considering a 223 ^{137}Cs activity of 740 GBq at different values of the distance D to the source along 224 the x-axis of irradiation field [6].	5-13
225 5.2	Correction factor c is computed thanks to formulae 5.5 taking as reference $D_0 =$ 226 50 cm and the associated flux F_0^{ABS} for each absorption factor available in table 5.1.	5-15
227 5.3	The data at D_0 in 1997 is taken from [6]. In a second step, using Equations 5.8 228 and 5.9, the flux at D can be estimated in 1997. Then, taking into account the 229 attenuation of the source activity, the flux at D can be estimated at the time of the 230 tests in GIF in 2014. Finally, assuming a sensitivity of the RPC to γ $s = 2 \cdot 10^{-3}$, 231 an estimation of the hit rate per unit area is obtained.	5-17
232 A.1	Inter-process communication cycles in between the webDCS and the DAQ through 233 file string signals.	A-15

234

List of Acronyms

235

List of Acronyms

236

237

A

238

239

240

AFL

Almost Full Level

241

242

B

243

244

245 BARC

Bhabha Atomic Research Centre

246 BLT

Block Transfer

247 BR

Branching Ratio

248

249

C

250

251

252 CAEN

Costruzioni Apparecchiature Elettroniche Nucleari S.p.A.

253 CERN

European Organization for Nuclear Research

254 CFD

Constant Fraction Discriminator

255 CMS

Compact Muon Solenoid

256 CSC

Cathode Strip Chamber

257

258

D

259

260

261 DAQ

Data Acquisition

262 DCS

Detector Control Software

263 DQM

Data Quality Monitoring

264 DT

Drift Tube

265

266

F

267

268

269	FEE	Front-End Electronics
270	FEB	Front-End Board
271		
272	G	
273		
274		
275	GE-/-	Find a good description
276	GE1/1	Find a good description
277	GE2/1	Find a good description
278	GEANT	GEometry ANd Tracking - a series of software toolkit platforms developed by CERN
279		
280	GEM	Gas Electron Multiplier
281	GIF	Gamma Irradiation Facility
282	GIF++	new Gamma Irradiation Facility
283		
284	H	
285		
286		
287	HL-LHC	High Luminosity LHC
288	HV	High Voltage
289		
290	I	
291		
292		
293	iRPC	improved RPC
294	IRQ	Interrupt Request
295		
296	L	
297		
298		
299	LHC	Large Hadron Collider
300	LS1	First Long Shutdown
301	LS3	Third Long Shutdown
302	LV	Low Voltage
303	LVDS	Low-Voltage Differential Signaling
304		
305	M	
306		
307		
308	MC	Monte Carlo
309	MCNP	Monte Carlo N-Particle
310	ME-/-	Find good description
311	ME0	Find good description

312	
313	
314	N
315	
316	NIM Nuclear Instrumentation Module logic signals
317	
318	
319	P
320	
321	PMT PhotoMultiplier Tube
322	
323	
324	R
325	
326	RE-/ Find a good description
327	RE2/2 Find a good description
328	RE3/1 Find a good description
329	RE3/2 Find a good description
330	RE4/1 Find a good description
331	RE4/2 Find a good description
332	RE4/3 Find a good description
333	RMS Root Mean Square
334	ROOT a framework for data processing born at CERN
335	RPC Resistive Plate Chamber
336	
337	
338	S
339	
340	SPS Super Proton Synchrotron
341	
342	
343	T
344	
345	TDC Time-to-Digital Converter
346	
347	
348	W
349	
350	webDCS Web Detector Control System

352

Nederlandse samenvatting –Summary in Dutch–

353

354 Le resume en Neerlandais (j'aurais peut-être de apprendre la langue juste pour ca...).

English summary

³⁵⁶ Le meme résume mais en Anglais (on commencera par la hein!).

1

Introduction

357

358

³⁵⁹ **1.1 A story of High Energy Physics**

³⁶⁰ **1.2 Organisation of this study**

2

361

362

Investigating the TeV scale

363 2.1 The Standard Model of Particle Physics

364 2.2 The Large Hadron Collider and the Compact Muon Solenoid

365 2.3 Muon Phase-II Upgrade

366 After the more than two years lasting First Long Shutdown (LS1), the Large Hadron Collider (LHC)
367 delivered its very first Run-II proton-proton collisions early 2015. LS1 gave the opportunity to the
368 LHC and to the its experiments to undergo upgrades. The accelerator is now providing collisions
369 at center-of-mass energy of 13 TeV and bunch crossing rate of 40 MHz, with a peak luminosity
370 exceeding its design value. During the first and upcoming second LHC Long Shutdown, the Compact
371 Muon Solenoid (CMS) detector is also undergoing a number of upgrades to maintain a high system
372 performance [1].

373 From the LHC Phase-2 or High Luminosity LHC (HL-LHC) period onwards, i.e. past the Third
374 Long Shutdown (LS3), the performance degradation due to integrated radiation as well as the average
375 number of inelastic collisions per bunch crossing, or pileup, will rise substantially and become a
376 major challenge for the LHC experiments, like CMS that are forced to address an upgrade program
377 for Phase-II [2]. Simulations of the expected distribution of absorbed dose in the CMS detector
378 under HL-LHC conditions, show in figure 5.14 that detectors placed close to the beamline will have
379 to withstand high irradiation, the radiation dose being of the order of a few tens of Gy.

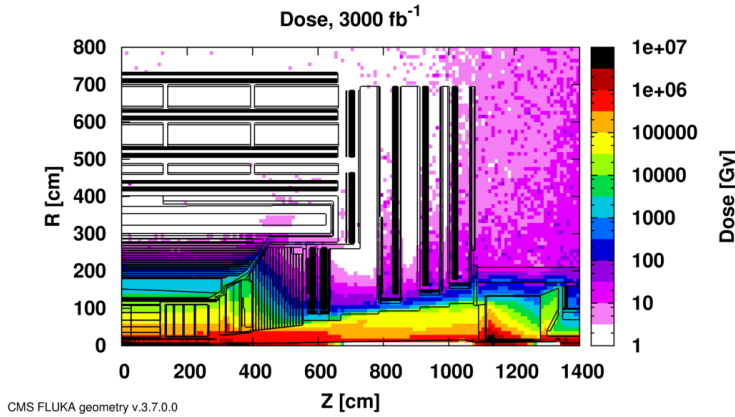


Figure 2.1: Absorbed dose in the CMS cavern after an integrated luminosity of 3000 fb⁻¹. R is the transverse distance from the beamline and Z is the distance along the beamline from the Interaction Point at Z=0.

The measurement of small production cross-section and/or decay branching ratio processes, such as the Higgs boson coupling to charge leptons or the $B_s \rightarrow \mu^+\mu^-$ decay, is of major interest and specific upgrades in the forward regions of the detector will be required to maximize the physics acceptance on the largest possible solid angle. To ensure proper trigger performance within the present coverage, the muon system will be completed with new chambers. In figure 2.2 one can see that the existing Cathode Strip Chambers (CSCs) will be completed by Gas Electron Multipliers (GEMs) and Resistive Plate Chambers (RPCs) in the pseudo-rapidity region $1.6 < |\eta| < 2.4$ to complete its redundancy as originally scheduled in the CMS Technical Proposal [3].

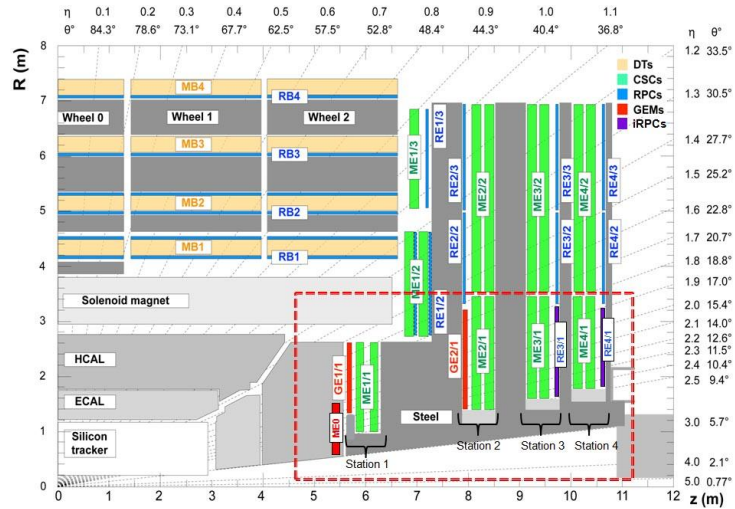


Figure 2.2: A quadrant of the muon system, showing DTs (yellow), RPCs (light blue), and CSCs (green). The locations of new forward muon detectors for Phase-II are contained within the dashed box and indicated in red for GEM stations (ME0, GE1/1, and GE2/1) and dark blue for improved RPC (iRPC) stations (RE3/1 and RE4/1).

RPCs are used by the CMS first level trigger for their good timing performances. Indeed, a very

good bunch crossing identification can be obtained with the present CMS RPC system, given their fast response of the order of 1 ns. In order to contribute to the precision of muon momentum measurements, muon chambers should have a spatial resolution less or comparable to the contribution of multiple scattering [1]. Most of the plausible physics is covered only considering muons with $p_T < 100$ GeV thus, in order to match CMS requirements, a spatial resolution of $\mathcal{O}(\text{few mm})$ the proposed new RPC stations, as shown by the simulation in figure 2.3. According to preliminary designs, RE3/1 and RE4/1 readout pitch will be comprised between 3 and 6 mm and 5 η -partitions could be considered.

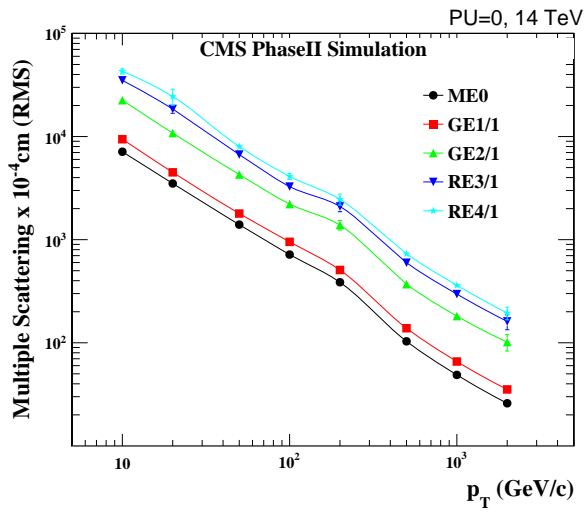


Figure 2.3: RMS of the multiple scattering displacement as a function of muon p_T for the proposed forward muon stations. All of the electromagnetic processes such as bremsstrahlung and magnetic field effect are included in the simulation.

3

397

398

Amplification processes in gaseous detectors

399

3.1 Signal formation

400

3.2 Gas transport parameters

4

401

402

Resistive Plate Chambers

403 **4.1 Principle**

404 **4.2 Rate capability of Resistive Plate Chambers**

405 **4.3 High time resolution**

406 **4.4 Resistive Plate Chambers at CMS**

407 **4.4.1 Overview**

408 The Resistive Plate Chambers (RPC) system, located in both barrel and endcap regions, provides a
409 fast, independent muon trigger with a looser p_T threshold over a large portion of the pseudorapidity
410 range ($|\eta| < 1.6$) [add reconstruction].

411

412 During High-Luminosity LHC (HL-LHC) operations the expected conditions in terms of back-
413 ground and pile-up will make the identification and correct P_T assignment a challenge for the Muon
414 system. The goal of RPC upgrade is to provide additional hits to the Muon system with precise tim-
415 ing. All these informations will be elaborated by the trigger system in a global way enhancing the
416 performance of the trigger in terms of efficiency and rate control. The RPC Upgrade is based on two
417 projects: an improved Link Board System and the extension of the RPC coverage up to $|\eta| = 2.4$.
418 [FIXME 2.4 or 2.5?]

419 The Link Board system, that will be described in section xxx, is responsible to process, syn-
420 chronize and zero-suppress the signals coming from the RPC front end boards. The Link Board
421 components have been produced between 2006 and 2007 and will be subjected to aging and failure
422 in the long term. The upgraded Link Board system will overcome the aging problems described in
423 section xxx and will allow for a more precise timing information to the RPC hits from 25 to 1 ns [ref
424 section xxx].

425 The extension of the RPC system up to $|\eta| = 2.1$ was already planned in the CMS TDR [ref
 426 cmstdr] and staged because of budget limitations and expected background rates higher than the rate
 427 capability of the present CMS RPCs in that region. An extensive R&D program has been done in
 428 order to develop an improved RPC that fulfills the CMS requirements. Two new RPC layers in the
 429 innermost ring of stations 3 and 4 will be added with benefits to the neutron-induced background
 430 reduction and efficiency improvement for both trigger and offline reconstruction.

431 4.4.2 The present RPC system

432 The RPC system is organized in 4 stations called RB1 to RB4 in the barrel region, and RE1 to RE4
 433 in the endcap region. The innermost barrel stations, RB1 and RB2, are instrumented with 2 layers
 434 of RPCs facing the innermost (RB1in and RB2in) and outermost (RB1out and RB2out) sides of the
 435 DT chambers. Every chamber is then divided from the read-out point of view into 2 or 3 η partitions
 436 called “rolls”. The RPC system consist of 480 barrel chambers and 576 endcap chambers. Details
 437 on the geometry are discussed in the paper [ref to geo paper].

438 The CMS RPC chamber is a double-gap, operated in avalanche mode to ensure reliable operation
 439 at high rates. Each RPC gap consists of two 2-mm-thick resistive High-Pressure Laminate (HPL)
 440 plates separated by a 2-mm-thick gas gap. The outer surface of the HPL plates is coated with a thin
 441 conductive graphite layer, and a voltage is applied. The RPCs are operated with a 3-component,
 442 non-flammable gas mixture consisting of 95.2% freon ($C_2H_2F_4$, known as R134a), 4.5% isobutane
 443 ($i-C_4H_{10}$), and 0.3% sulphur hexafluoride (SF_6) with a relative humidity of 40% - 50%. Readout
 444 strips are aligned in η between the 2 gas gaps. [\[Add a sentence on FEBs.\]](#)

445 The discriminated signals coming from the Front End boards feed via twisted cables (10 to 20 m
 446 long) the Link Board System located in UXC on the balconies around the detector. The Link System
 447 consist of the 1376 Link Boards (LBs) and the 216 Control Boards (CBs), placed in 108 Link Boxes.
 448 The Link Box is a custom crate (6U high) with 20 slots (for two CBs and eighteen LBs). The Link
 449 Box contains custom backplane to which the cables from the chambers are connected, as well as the
 450 cables providing the LBs and CBs power supply and the cables for the RPC FEBs control with use
 451 of the I2C protocol (trough the CB). The backplane itself contains only connectors (and no any other
 452 electronic devices).

453 The Link Board has 96 input channels (one channel corresponds to one RPC strip). The input
 454 signals are the ~ 100 ns binary pulses which are synchronous to the RPC hits, but not to the LHC
 455 clock (which drives the entire CMS electronics). Thus the first step of the FEB signals processing
 456 is synchronization, i.e. assignment of the signals to the BXes (25 ns periods). Then the data are
 457 compressed with a simple zero-suppressing algorithm (the input channels are grouped into 8 bit
 458 partitions, only the partitions with at least one nonzero bit are selected for each BX). Next, the non-
 459 empty partitions are time-multiplexed i.e. if there are more than one such partition in a given BX,
 460 they are sent one-by-one in consecutive BXes. The data from 3 neighbouring LBs are concentrated
 461 by the middle LB which contains the optical transmitter for sending them to the USC over a fiber at
 462 1.6 Gbps.

463 The Control Boards provide the communication of the control software with the LBs via the
 464 FEC/CCU system. The CBs are connected into token rings, each ring consists of 12 CBs of one
 465 detector tower and a FEC mezzanine board placed on the CCS board located in the VME crate in
 466 the USC. In total, there are 18 rings in the entire Link System. The CBs also perform automatic
 467 reloading of the LB's firmware which is needed in order to avoid accumulation of the radiation
 468 induced SEUs in the LBs firmware.

469 Both LBs and CB are based on the Xilinx Spartan III FPGAs, the CB additionally contains
 470 radiation-tolerant (FLASH based) FPGA Actel ProAsicPlus.

471 The High Voltage power system is located in USC, not exposed to radiation and easily accessible
 472 for any reparation. A single HV channel powers 2 RPC chambers both in the barrel and endcap
 473 regions. The Low Voltage boards are located in UXC on the balconies and provide the voltage to the
 474 front end electronics.

475 4.4.3 Pulse processing of CMS RPCs

476 Signals induced by cosmic particle in the RPC strips are shaped by standard CMS RPC Front-End
 477 Electronics (FEE) following the scheme of Figure 4.1. On a first stage, analogic signals are amplified
 478 and then sent to the Constant Fraction Discriminator (CFD) described in Figure 4.2. At the end of
 479 the chain, 100 ns long pulses are sent in the LVDS output. These output signal are sent on one side to
 480 a V1190A Time-to-Digital Converter (TDC) module from CAEN and on the other to an OR module
 481 to count the number of detected signals. Trigger and hit coïncidences are monitored using scalers.
 482 The TDC is used to store the data into ROOT files. These files are thus analysed to understand the
 483 detectors performance.

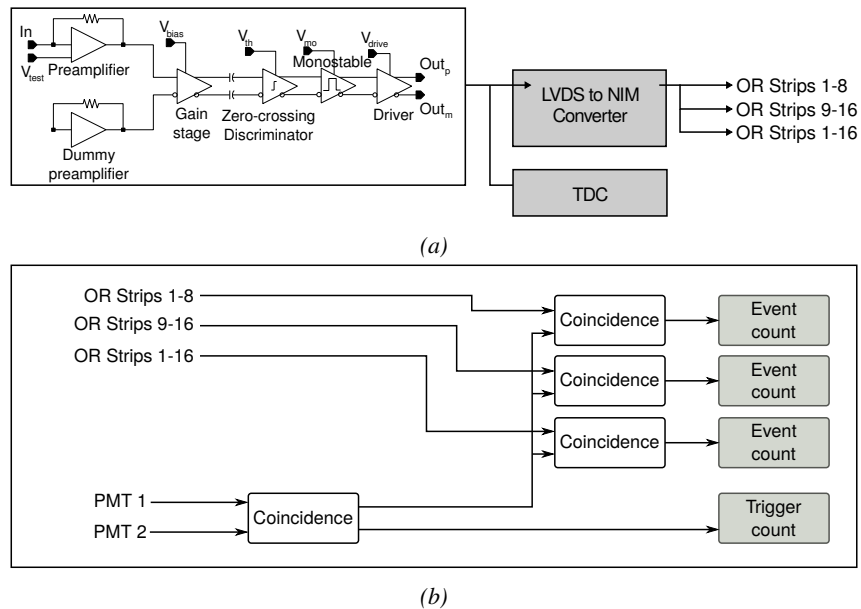


Figure 4.1: Signals from the RPC strips are shaped by the FEE described on Figure 4.1a. Output LVDS signals are then read-out by a TDC module connected to a computer or converted into NIM and sent to scalers. Figure 4.1b describes how these converted signals are put in coincidence with the trigger.

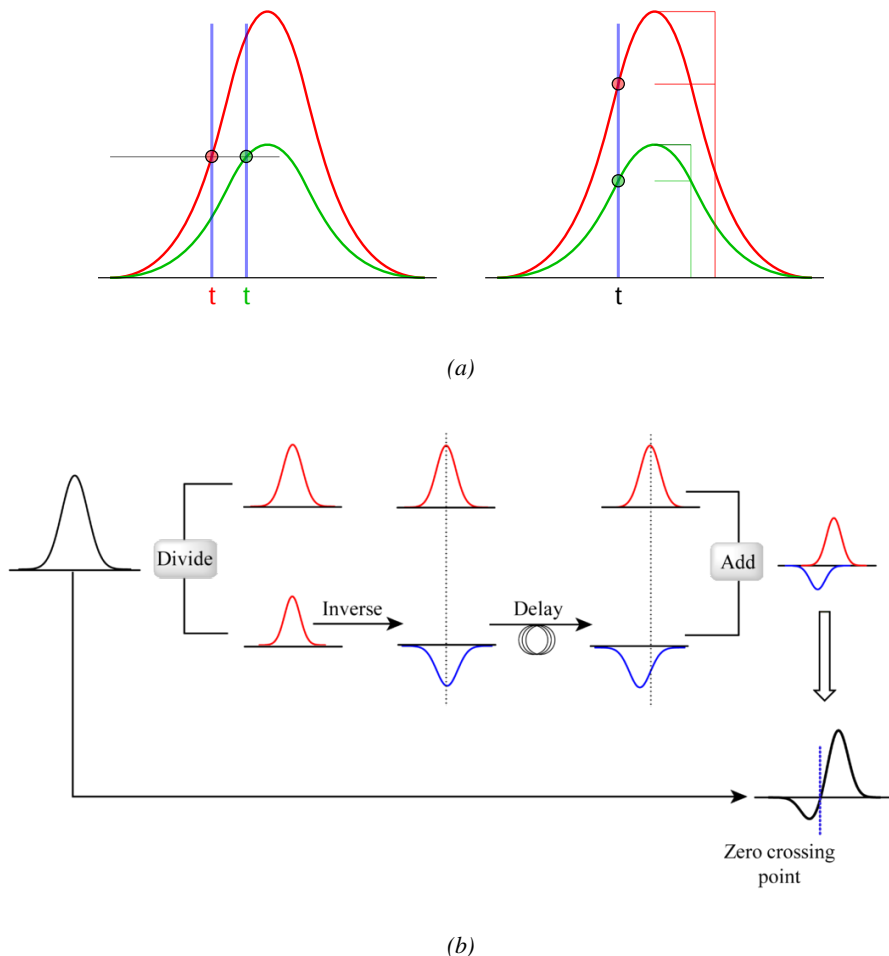


Figure 4.2: Description of the principle of a CFD. A comparison of threshold triggering (left) and constant fraction triggering (right) is shown in Figure 4.2a. Constant fraction triggering is obtained thanks to zero-crossing technique as explained in Figure 4.2b. The signal arriving at the input of the CFD is split into three components. A first one is delayed and connected to the inverting input of a first comparator. A second component is connected to the noninverting input of this first comparator. A third component is connected to the noninverting input of another comparator along with a threshold value connected to the inverting input. Finally, the output of both comparators is fed through an AND gate.

5

484

485

486

Longevity studies and Consolidation of the present CMS RPC subsystem

487

5.1 Testing detectors under extreme conditions

488

The upgrade from LHC to HL-LHC will increase the peak luminosity from $10^{34} \text{ cm}^{-2} \text{ s}^{-1}$ to reach $5 \times 10^{34} \text{ cm}^{-2} \text{ s}^{-1}$, increasing in the same way the total expected background to which the RPC system will be subjected to. Composed of low energy gammas and neutrons from $p\text{-}p$ collisions, low momentum primary and secondary muons, puch-through hadrons from calorimeters, and particles produced in the interaction of the beams with collimators, the background will mostly affect the regions of CMS that are the closest to the beam line, i.e. the RPC detectors located in the endcaps.

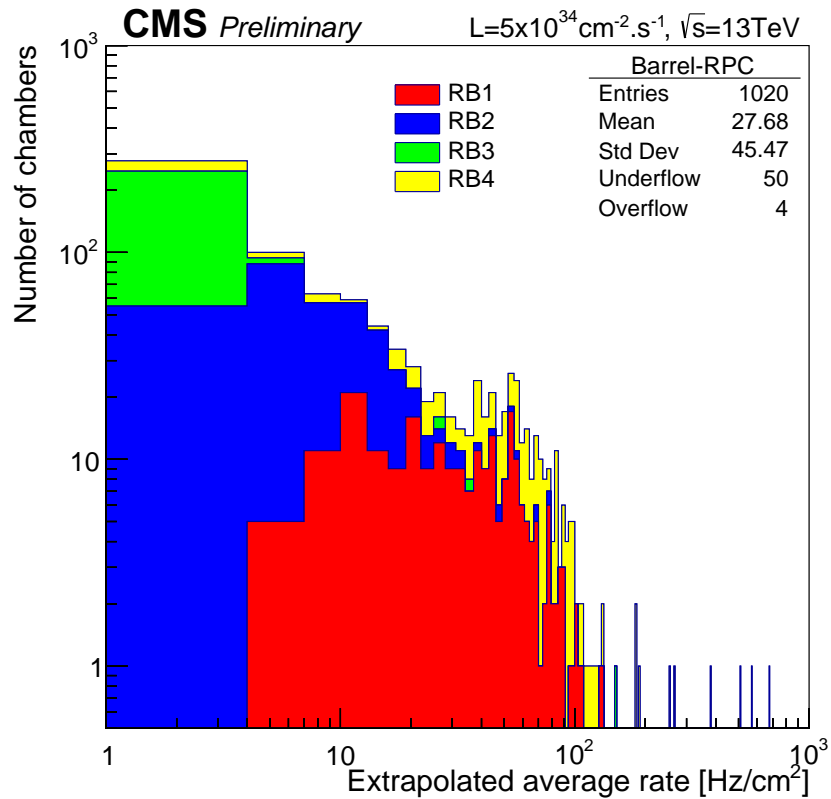
[To update.]

495

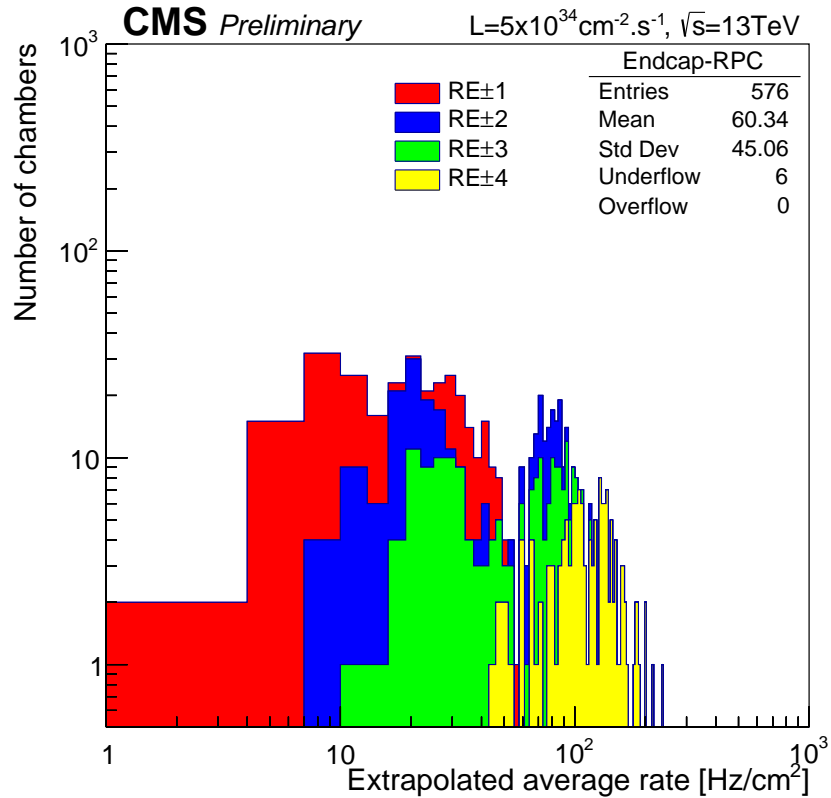
496

The 2016 data allowed to study the values of the background rate in all RPC system. In Figure 5.1, the distribution of the chamber background hit rate per unit area is shown at a luminosity of $5 \times 10^{34} \text{ cm}^{-2} \cdot \text{s}^{-1}$ linearly extrapolating from data collected in 2016 [ref mentioning the linear dependency of rate vs lumi]. The maximum rate per unit area at HL-LHC conditions is expected to be of the order of 600 Hz/cm^2 (including a safety factor 3). Nevertheless, Fluka simulations have conducted in order to understand the background at HL-LHC conditions. The comparison to the data has shown, in Figure 5.2, a discrepancy of a factor 2 even though the order of magnitude is consistent. [Understand mismatch.]

504



(a)



(b)

Figure 5.1: (5.1a) Extrapolation from 2016 data of single hit rate per unit area in the barrel region. (5.1b) Extrapolation from 2016 data of single hit rate per unit area in the endcap region.

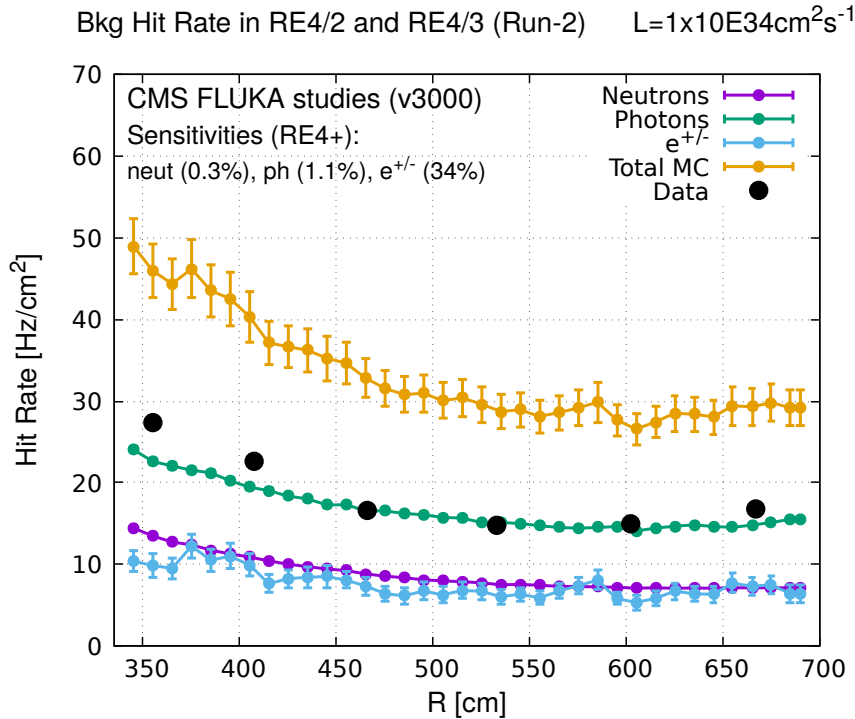


Figure 5.2: Background Fluka simulation compared to 2016 Data at $L = 10^{34} \text{ cm}^{-2} \cdot \text{s}^{-1}$ in the fourth endcap disk region. A mismatch in between simulation and data can be observed. [\[To be understood.\]](#)

505 In the past, extensive long-term tests were carried out at several gamma and neutron facilities
 506 certifying the detector performance. Both full size and small prototype RPCs have been irradiated
 507 with photons up to an integrated charge of $\sim 0.05 \text{ C/cm}^2$ and $\sim 0.4 \text{ C/cm}^2$, respectively [4, 5].
 508 During Run-I, the RPC system provided stable operation and excellent performance and did not
 509 show any aging effects for integrated charge of the order of 0.01 C/cm^2 . Projections on currents
 510 from 2016 Data, has allowed to determine that the total integrated charge, by the end of HL-LHC,
 511 would be of the order of 1 C/cm^2 (including a safety factor 3). [\[Corresponding figure needed.\]](#)
 512

513 5.1.1 The Gamma Irradiation Facilities

514 5.1.1.1 GIF

515 Located in the SPS West Area at the downstream end of the X5 test beam, the Gamma Irradiation
 516 Facility (GIF) was a test area in which particle detectors were exposed to a particle beam in presence
 517 of an adjustable gamma background [6]. Its goal was to reproduce background conditions these
 518 detectors would suffer in their operating environment at LHC. GIF layout is shown in Figure 5.3.
 519 Gamma photons are produced by a strong ^{137}Cs source installed in the upstream part of the zone
 520 inside a lead container. The source container includes a collimator, designed to irradiate a $6 \times 6 \text{ m}^2$
 521 area at 5 m maximum to the source. A thin lens-shaped lead filter helps providing with a uniform
 522 outcoming flux in a vertical plane, orthogonal to the beam direction. The principal collimator hole
 523 provides a pyramidal aperture of $74^\circ \times 74^\circ$ solid angle and provides a photon flux in a pyramidal vol-

ume along the beam axis. The photon rate is controled by further lead filters allowing the maximum rate to be limited and to vary within a range of four orders of magnitude. Particle detectors under test are then placed within the pyramidal volume in front of the source, perpendicularly to the beam line in order to profit from the homogeneous photon flux. Adjusting the background flux of photons can then be done by using the filters and choosing the position of the detectors with respect to the source.

529

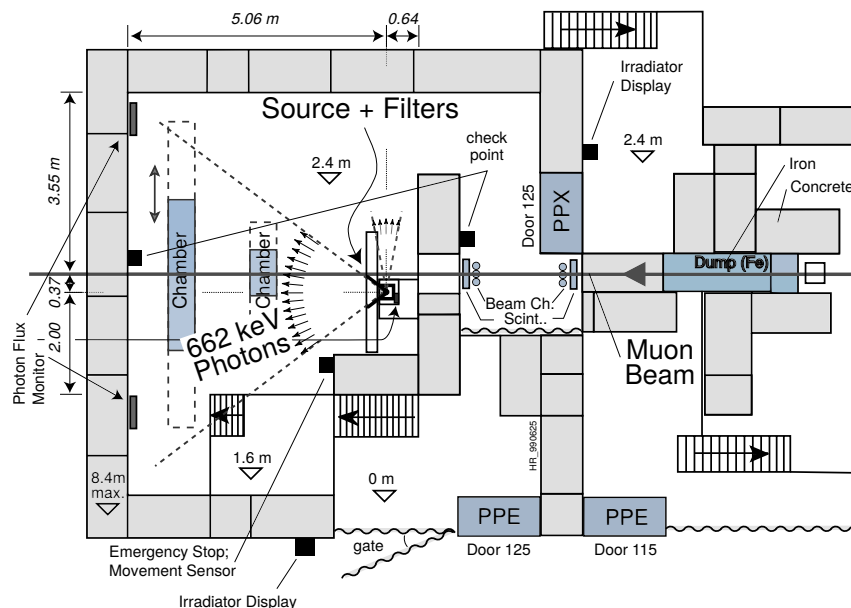


Figure 5.3: Layout of the test beam zone called X5c GIF at CERN. Photons from the radioactive source produce a sustained high rate of random hits over the whole area. The zone is surrounded by 8 m high and 80 cm thick concrete walls. Access is possible through three entry points. Two access doors for personnel and one large gate for material. A crane allows installation of heavy equipment in the area.

530 As described on Figure 5.4, the ^{137}Cs source emits a 662 keV photon in 85% of the decays. An
 531 activity of 740 GBq was measured on the 5th March 1997. To estimate the strength of the flux in
 532 2014, it is necessary to consider the nuclear decay through time assiciated to the Cesium source
 533 whose half-life is well known ($t_{1/2} = (30.05 \pm 0.08)$ y). The GIF tests where done in between the
 534 20th and the 31st of August 2014, i.e. at a time $t = (17.47 \pm 0.02)$ y resulting in an attenuation of
 535 the activity from 740 GBq in 1997 to 494 GBq in 2014.

536

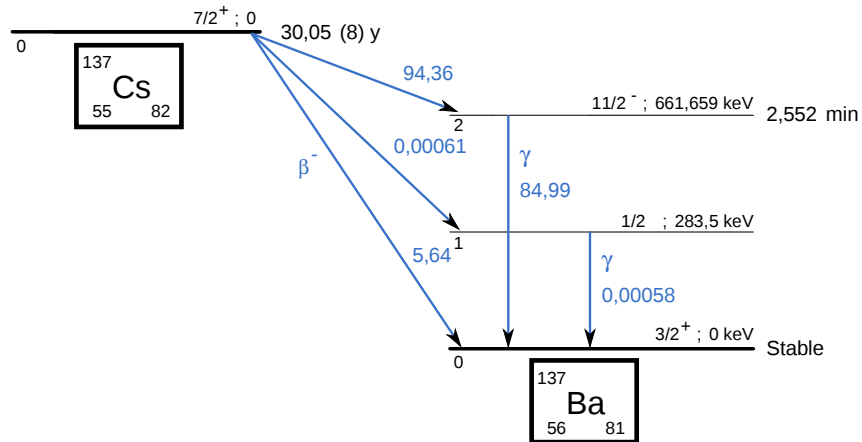


Figure 5.4: ^{137}Cs decays by β^- emission to the ground state of ^{137}Ba ($\text{BR} = 5.64\%$) and via the 662 keV isomeric level of ^{137}Ba ($\text{BR} = 94.36\%$) whose half-life is 2.55 min.

5.1.1.2 GIF++

The new Gamma Irradiation Facility (GIF++), located in the SPS North Area at the downstream end of the H4 test beam, has replaced its predecessor during LS1 and has been operational since spring 2015 [7]. Like GIF, GIF++ features a ^{137}Cs source of 662 keV gamma photons, their fluence being controlled with a set of filters of various attenuation factors. The source provides two separated large irradiation areas for testing several full-size muon detectors with continuous homogeneous irradiation, as presented in Figure 5.5.

544

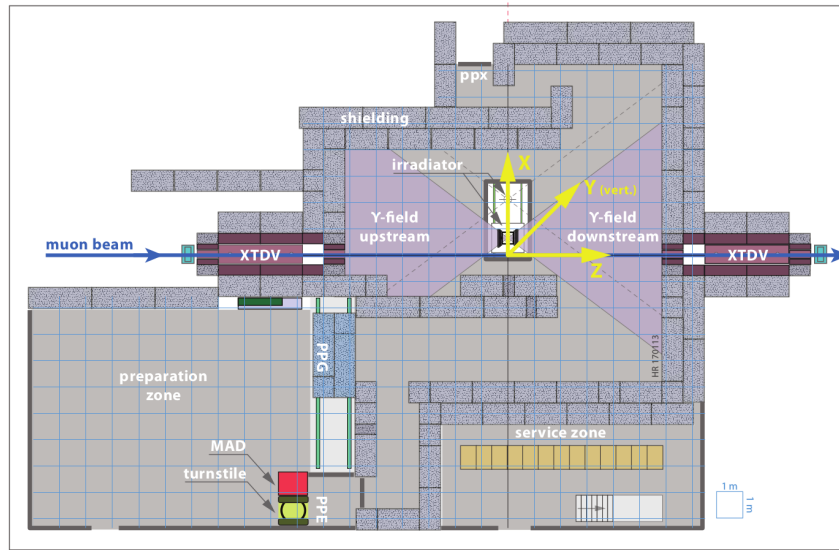


Figure 5.5: Floor plan of the GIF++ facility. When the facility downstream of the GIF++ takes electron beam, a beam pipe is installed along the beam line (z -axis). The irradiator can be displaced laterally (its center moves from $x = 0.65 \text{ m}$ to 2.15 m), to increase the distance to the beam pipe.

545 The source activity was measured to be about 13.5 TBq in March 2016. The photon flux being
 546 far greater than HL-LHC expectations, GIF++ provides an excellent facility for accelerated aging
 547 tests of muon detectors.

548

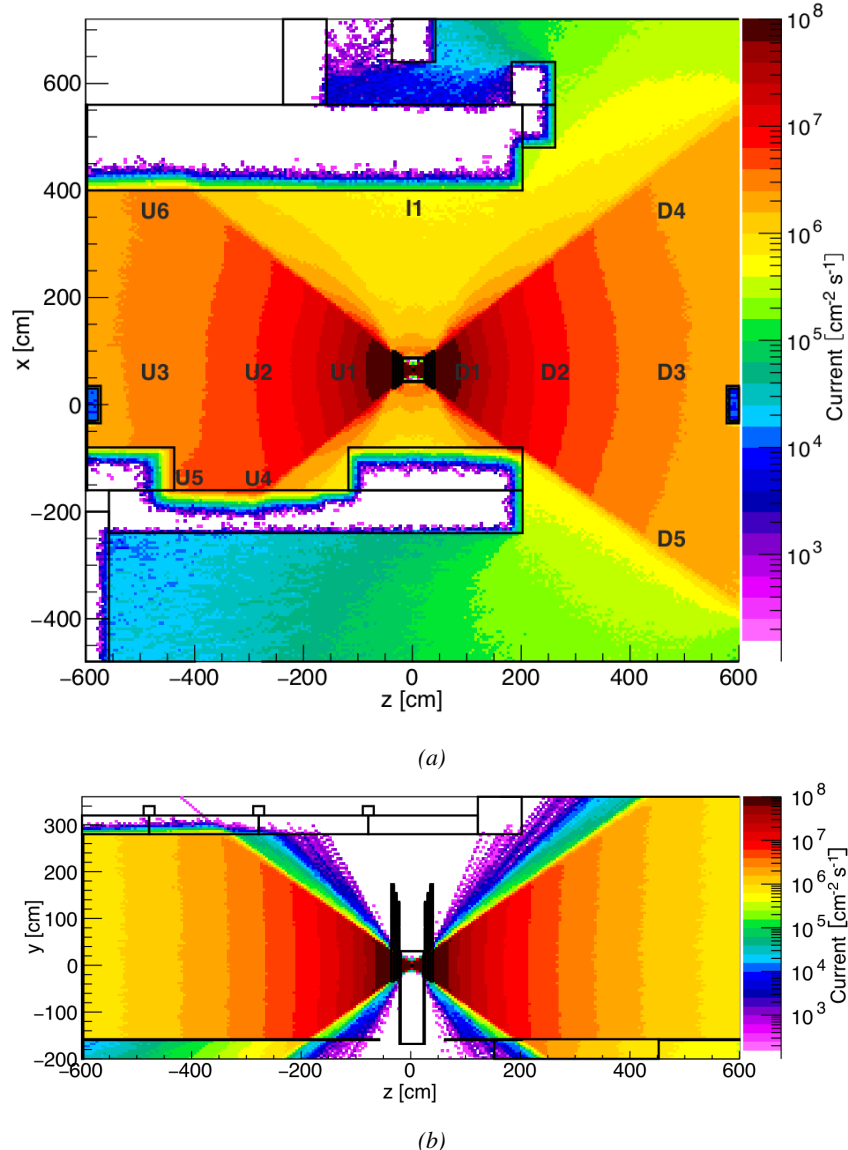


Figure 5.6: Simulated unattenuated current of photons in the xz plane (Figure 5.6a) and yz plane (Figure 5.6b) through the source at $x = 0.65$ m and $y = 0$ m. With angular correction filters, the current of 662 keV photons is made uniform in xy planes.

549 The source is situated in the muon beam line with the muon beam being available a few times a
 550 year. The H4 beam, composed of muons with a momentum of about 150 GeV/c, passes through the
 551 GIF++ zone and is used to study the performance of the detectors. Its flux is of 104 particles/ s cm^2

552 focused in an area similar to $10 \times 10 \text{ cm}^2$. Therefore, with properly adjusted filters, one can imitate
 553 the HL-LHC background and study the performance of muon detectors with their trigger/readout
 554 electronics in HL-LHC environment.

555

556 5.2 Preliminary tests at GIF

557 5.2.1 Resistive Plate Chamber test setup

558 During summer 2014, preliminary tests have been conducted in the GIF area on a newly produced
 559 RE4/2 chamber labelled RE-4-2-BARC-161. This chamber has been placed into a trolley covered
 560 with a tent. The position of the RPC inside the tent and of the tent related to the source is described
 561 in Figure 5.7. To test this CMS RPC, three different absorber settings were used. First of all,
 562 measurements were done with fully opened source. Then, to complete this preliminary study, the
 563 gamma flux has been attenuated from a factor 2 and a factor 5. The expected gamma flux at the level
 564 of our detector will be discussed in subsection ??.

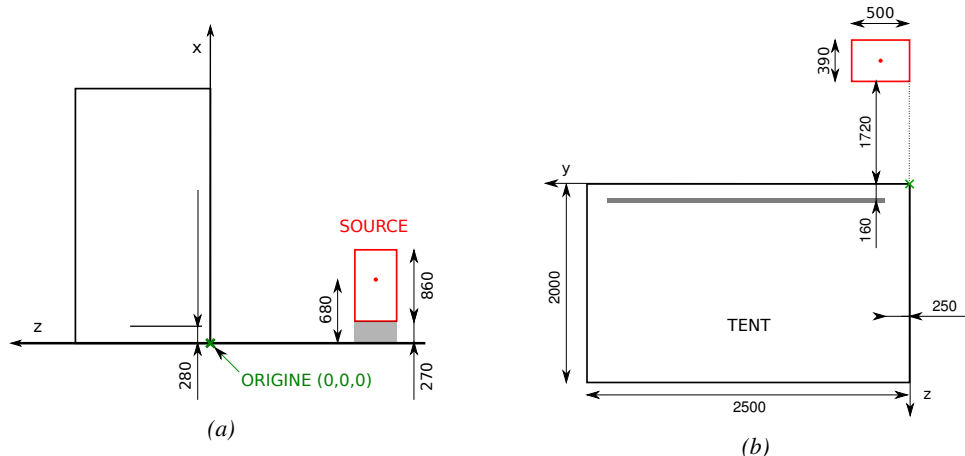


Figure 5.7: Description of the RPC setup. Dimensions are given in mm. A tent containing RPCs is placed at 1720 mm from the source container. The source is situated in the center of the container. RE-4-2-BARC-161 chamber is 160 mm inside the tent. This way, the distance between the source and the chambers plan is 2060 mm. Figure 5.7a provides a side view of the setup in the xz plane while Figure 5.7b shows a top view in the yz plane.



Figure 5.8: RE-4-2-BARC-161 chamber is inside the tent as described in Figure 5.7. In the top right, the two scintillators used as trigger can be seen. This trigger system has an inclination of 10° relative to horizontal and is placed above half-partition B2 of the RPCs. PMT electronics are shielded thanks to lead blocks placed in order to protect them without stopping photons from going through the scintillators and the chamber.

565 At the time of the tests, the beam not being operational anymore, a trigger composed of 2
 566 plastic scintillators has been placed in front of the setup with an inclination of 10 deg with respect to
 567 the detector plane in order to look at cosmic muons. Using this particular trigger layout, shown on
 568 Figure 5.8, leads to a cosmic muon hit distribution into the chamber similar to the one in Figure 5.9.
 569 Measured without gamma irradiation, two peaks can be seen on the profil of partition B, centered
 570 on strips 52 and 59. Section ?? will help us understand that these two peaks are due respectively to
 571 forward and backward coming cosmic particles where forward coming particles are first detected by
 572 the scintillators and then the RPC while the backward coming muons are first detected in the RPC.

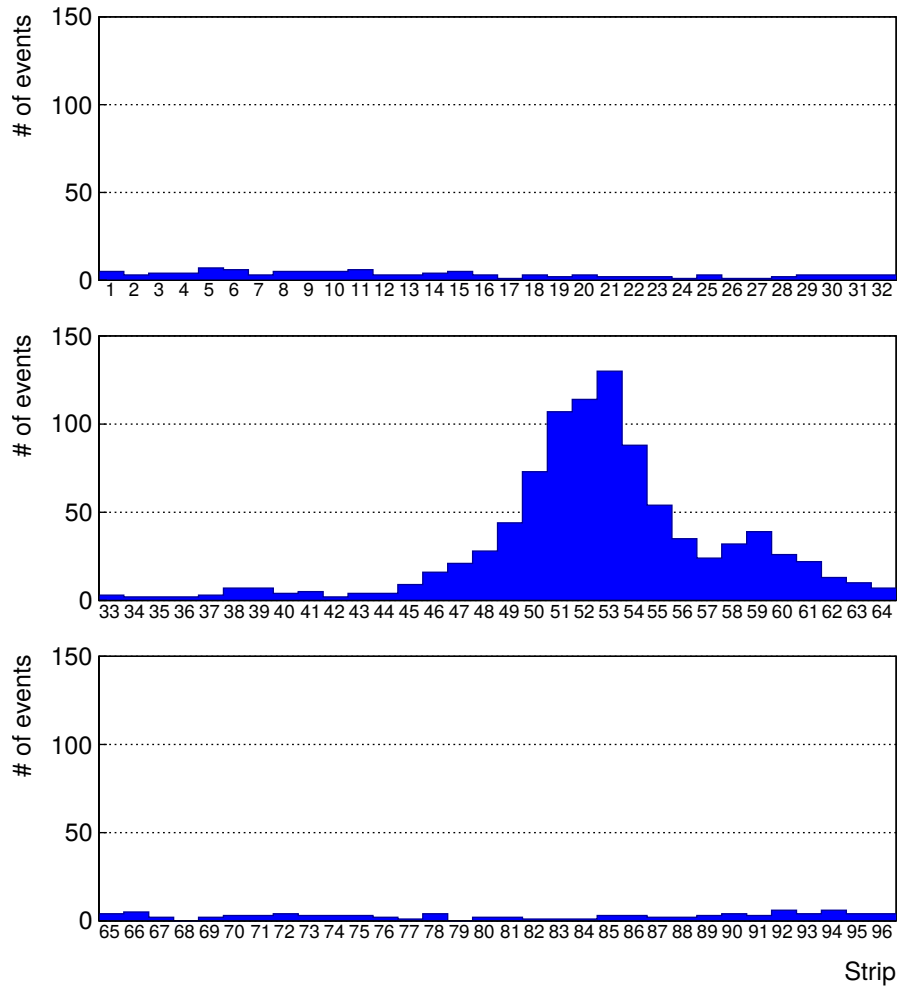


Figure 5.9: Hit distributions over all 3 partitions of RE-4-2-BARC-161 chamber is showed on these plots. Top, middle and bottom figures respectively correspond to partitions A, B, and C. These plots show that some events still occur in other half-partitions than B2, which corresponds to strips 49 to 64, in front of which the trigger is placed, contributing to the inefficiency of detection of cosmic muons. In the case of partitions A and C, the very low amount of data can be interpreted as noise. On the other hand, it is clear that a little portion of muons reach the half-partition B1, corresponding to strips 33 to 48.

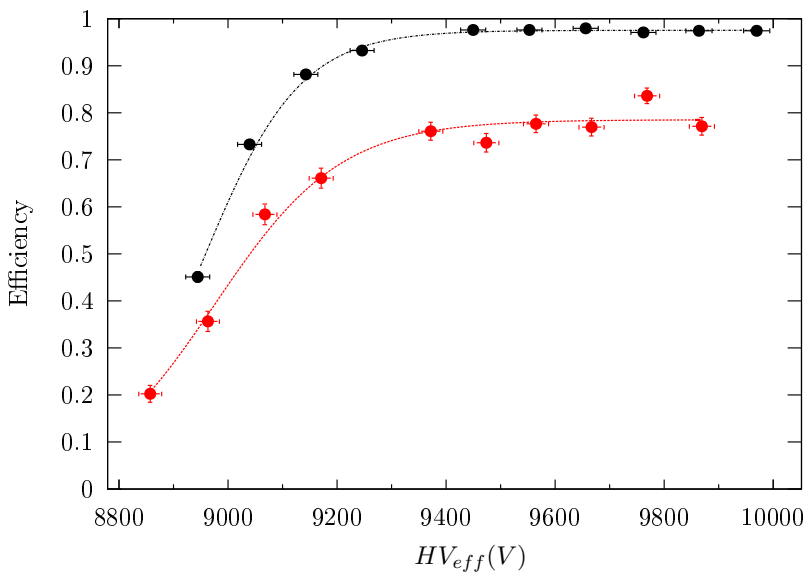
573 5.2.2 Data Acquisition

574 5.2.3 Geometrical acceptance of the setup layout to cosmic muons

575 In order to profit from a constant gamma irradiation, the detectors inside of the GIF bunker need
 576 to be placed in a plane orthogonal to the beam line. The muon beam that used to be available was
 577 meant to test the performance of detectors under test. This beam not being active anymore, another
 578 solution to test detector performance had to be used. Thus, it has been decided to use cosmic muons
 579 detected through a telescope composed of two scintillators. Lead blocks were used as shielding to

580 protect the photomultipliers from gammas as can be seen from Figure 5.8.

581 An inclination has been given to the cosmic telescope to maximize the muon flux. A good com-
 582 promise had to be found between good enough muon flux and narrow enough hit distribution to
 583 be sure to contain all the events into only one half partitions as required from the limited available
 584 readout hardware. Nevertheless, a consequence of the misplaced trigger, that can be seen as a loss
 585 of events in half-partition B1 in Figure 5.9, is an inefficiency. Nevertheless, the inefficiency of ap-
 586 proximately 20 % highlighted in Figure 5.10 by comparing the performance of chamber BARC-161
 587 in 904 and at GIF without irradiation seems too important to be explained only by the geometri-
 588 cal acceptance of the setup itself. Simulations have been conducted to show how the setup brings
 589 inefficiency.



590 *Figure 5.10: Results are derived from data taken on half-partition B2 only. On the 18th of June 2014, data
 591 has been taken on chamber RE-2-BARC-161 at building 904 (Prevessin Site) with cosmic muons providing us a
 592 reference efficiency plateau of $(97.54 \pm 0.15)\%$ represented by a black curve. A similar measurement has been
 593 done at GIF on the 21st of July with the same chamber giving a plateau of $(78.52 \pm 0.94)\%$ represented by a
 594 red curve.*

595 5.2.3.1 Description of the simulation layout

596 The layout of GIF setup has been reproduced and incorporated into a Monte Carlo (MC) simulation
 597 to study the influence of the disposition of the telescope on the final distribution measured by the
 598 RPC. A 3D view of the simulated layout is given into Figure 5.11. Muons are generated randomly
 599 in a horizontal plane located at a height corresponding to the lowest point of the PMTs. This way,
 600 the needed size of the plane in order to simulate events happening at very big azimuthal angles (i.e.
 $\theta \approx \pi$) can be kept relatively small. The muon flux is designed to follow the usual $\cos^2\theta$ distribution
 for cosmic particle. The goal of the simulation is to look at muons that pass through the muon
 telescope composed of the two scintillators and define their distribution onto the RPC plane. During
 the reconstruction, the RPC plane is then divided into its strips and each muon track is assigned to a
 strip.

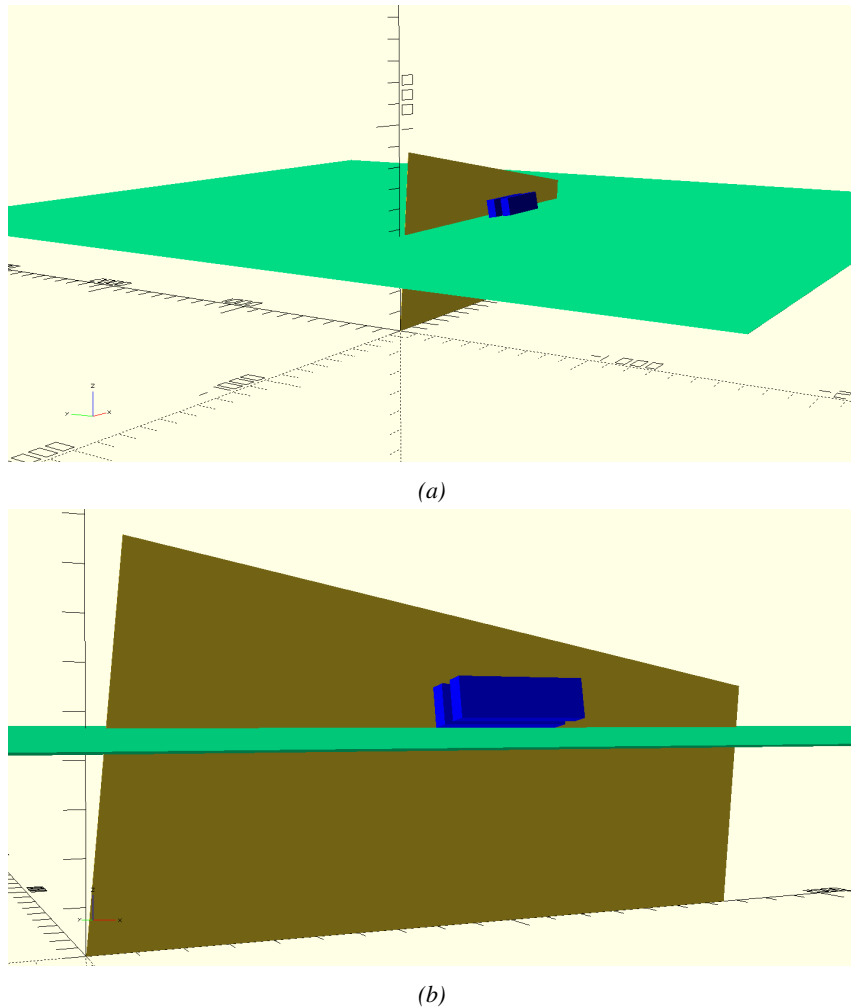


Figure 5.11: Representation of the layout used for the simulations of the test setup. The RPC is represented as a yellow trapezoid while the two scintillators as blue cuboids looking at the sky. A green plane corresponds to the muon generation plane within the simulation. Figure 5.7a shows a global view of the simulated setup. Figure 5.7b shows a zoomed view that allows to see the 2 scintillators as well as the full RPC plane.

601 In order to further refine the quality of the simulation and understand deeper the results the
 602 dependance of the distribution has been studied for a range of telescope inclinations. Moreover,
 603 the threshold applied on the PMT signals has been included into the simulation in the form of a
 604 cut. In the approximation of uniform scintillators, it has been considered that the threshold can be
 605 understood as the minimum distance particles need to travel through the scintillating material to give
 606 a strong enough signal. Particles that travel a distance smaller than the set "threshold" are thus not
 607 detected by the telescope and cannot trigger the data taking. Finally, the FEE threshold also has
 608 been considered in a similar way. The mean momentum of horizontal cosmic rays is higher than
 609 those of vertical ones but the stopping power of matter for momenta ranging from 1 GeV to 1 TeV
 610 stays comparable. It is then possible to assume that the mean number of primary e^-/ion pairs per
 611 unit length will stay similar and thus, depending on the applied discriminator threshold, muons with

612 the shortest path through the gas volume will deposit less charge and induce a smaller signal on the
 613 pick-up strips that could eventually not be detected. These two thresholds also restrain the overall
 614 geometrical acceptance of the system.

615 **5.2.3.2 Simulation procedure**

616 The simulation software has been designed using C++ and the output data is saved into ROOT
 617 histograms. Simulations start for a threshold T_{scint} varying in a range from 0 to 45 mm in steps
 618 of 5 mm, where $T_{scint} = 0$ mm corresponds to the case where there isn't any threshold apply on
 619 the input signal while $T_{scint} = 45$ mm, which is the scintillator thickness, is the case where muons
 620 cannot arrive orthogonally onto the scintillator surface. For a given T_{scint} , a set of RPC thresholds
 621 are considered. The RPC threshold, T_{RPC} varies from 2 mm, the thickness of the gas volume, to
 622 3 mm in steps of 0.25 mm. For each $(T_{scint}; T_{RPC})$ pair, $N_\mu = 10^8$ muons are randomly generated
 623 inside the muon plane described in the previous paragraph with an azimuthal angle θ chosen to follow
 624 a $\cos^2\theta$ distribution.

625 Planes are associated to each surface of the scintillators. Knowing muon position into the muon
 626 plane and its direction allows us, by assuming that muons travel in a straight line, to compute the
 627 intersection of the muon track with these planes. Applying conditions to the limits of the surfaces
 628 of the scintillator faces then gives us an answer to whether or not the muon passed through the
 629 scintillators. In the case the muon has indeed passed through the telescope, the path through each
 630 scintillator is computed and muons whose path was shorter than T_{scint} are rejected and are thus
 631 considered as having not interacted with the setup.

632 On the contrary, if the muon is labeled as good, its position within the RPC plane is computed
 633 and the corresponding strip, determined by geometrical tests in the case the distance through the
 634 gas volume was enough not to be rejected because of T_{RPC} , gets a hit and several histograms
 635 are filled in order to keep track of the generation point on the muon plane, the intersection points
 636 of the reconstructed muons within the telescope, or on the RPC plane, the path traveled through
 637 each individual scintillator or the gas volume, as well as other histograms. Moreover, muons fill
 638 different histograms whether they are forward or backward coming muons. They are discriminated
 639 according to their direction components. When a muon is generated, an (x, y, z) position is assigned
 640 into the muon plane as well as a $(\theta; \phi)$ pair that gives us the direction it's coming from. This way,
 641 muons satisfying the condition $0 \leq \phi < \pi$ are designated as backward coming muons while muons
 642 satisfying $\pi \leq \phi < 2\pi$ as forward coming muons.

643 This simulation is then repeated for different telescope inclinations ranging in between 4 and 20°
 644 and varying in steps of 2° . Due to this inclination and to the vertical position of the detector under
 645 test, the muon distribution reconstructed in the detector plane is asymmetrical. The choice as been
 646 made to chose a skew distribution formula to fit the data built as the multiplication of gaussian and
 647 sigmoidal curves together. A typical gaussian formula is given as 5.1 and has three free parameters
 648 as A_g , its amplitude, \bar{x} , its mean value and σ , its root mean square. Sigmoidal curves as given by
 649 formula 5.2 are functions converging to 0 and A_s as x diverges. The inflection point is given as x_i
 650 and λ is proportional to the slope at $x = x_i$. In the limit where $\lambda \rightarrow \infty$, the sigmoid becomes a
 651 step function.

$$g(x) = A_g e^{-\frac{(x-\bar{x})^2}{2\sigma^2}} \quad (5.1)$$

$$s(x) = \frac{A_s}{1 + e^{-\lambda(x-x_i)}} \quad (5.2)$$

652 Finally, a possible representation of a skew distribution is given by formula 5.3 and is the product
 653 of 5.1 and 5.2. Naturally, here $A_{sk} = A_g \times A_s$ and represents the theoretical maximum in the limit
 654 where the skew tends to a gaussian function.

$$sk(x) = g(x) \times s(x) = A_{sk} \frac{e^{\frac{-(x-\bar{x})^2}{2\sigma^2}}}{1 + e^{-\lambda(x-x_i)}} \quad (5.3)$$

655 **5.2.3.3 Results**

656 **Influence of T_{scint} on the muon distribution**

657 **Influence of T_{RPC} on the muon distribution**

658 **Influence of the telescope inclination on the muon distribution**

659 **Comparison to data taken at GIF without irradiation**

660 **5.2.4 Photon flux at GIF**

661 **5.2.4.1 Expectations from simulations**

662 In order to understand and evaluate the γ flux in the GIF area, simulations had been conducted in
 663 1999 and published by S. Agosteo et al [6]. Table 5.1 presented in this article gives us the γ flux
 664 for different distances D to the source. This simulation was done using GEANT and a Monte Carlo
 665 N-Particle (MCNP) transport code, and the flux F is given in number of γ per unit area and unit time
 666 along with the estimated error from these packages expressed in %.

Nominal ABS	Photon flux F [$s^{-1}cm^{-2}$]			
	at $D = 50$ cm	at $D = 155$ cm	at $D = 300$ cm	at $D = 400$ cm
1	$0.12 \cdot 10^8 \pm 0.2\%$	$0.14 \cdot 10^7 \pm 0.5\%$	$0.45 \cdot 10^6 \pm 0.5\%$	$0.28 \cdot 10^6 \pm 0.5\%$
2	$0.68 \cdot 10^7 \pm 0.3\%$	$0.80 \cdot 10^6 \pm 0.8\%$	$0.25 \cdot 10^6 \pm 0.8\%$	$0.16 \cdot 10^6 \pm 0.6\%$
5	$0.31 \cdot 10^7 \pm 0.4\%$	$0.36 \cdot 10^6 \pm 1.2\%$	$0.11 \cdot 10^6 \pm 1.2\%$	$0.70 \cdot 10^5 \pm 0.9\%$

Table 5.1: Total photon flux ($E\gamma \leq 662$ keV) with statistical error predicted considering a ^{137}Cs activity of 740 GBq at different values of the distance D to the source along the x -axis of irradiation field [6].

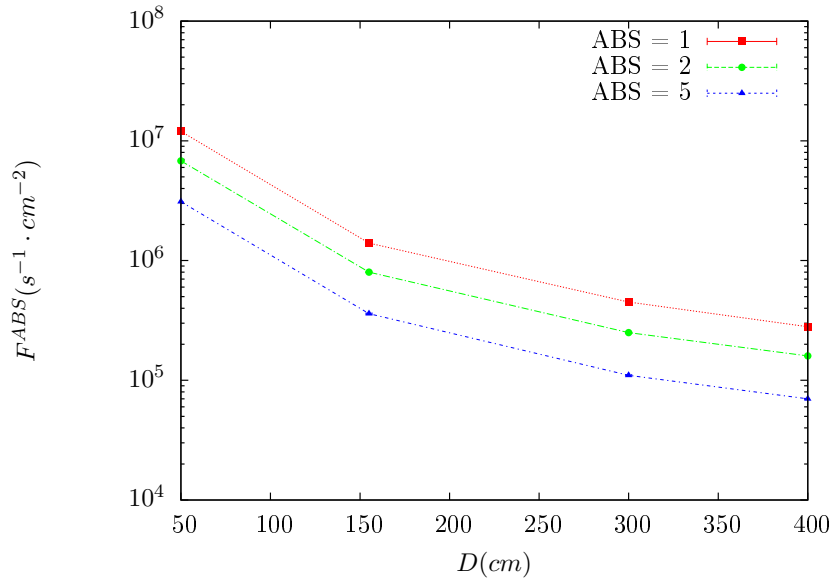


Figure 5.12: γ flux $F(D)$ is plot using values from table 5.1. As expected, the plot shows similar attenuation behaviours with increasing distance for each absorption factors.

The simulation doesn't directly provides us with an estimated flux at the level of our RPC. First of all, it is needed to extract the value of the flux from the available data contained in the original paper and then to estimate the flux in 2014 at the time the experimentation took place. Figure 5.12 that contains the data from Table 5.1. In the case of a pointlike source emitting isotropic and homogeneous gamma radiations, the gamma flux F at a distance D to the source with respect to a reference point situated at D_0 where a known flux F_0 is measured will be expressed like in Equation 5.4, assuming that the flux decreases as $1/D^2$, where c is a fitting factor.

$$F^{ABS} = F_0^{ABS} \times \left(\frac{cD_0}{D} \right)^2 \quad (5.4)$$

By rewriting Equation 5.4, it comes that :

$$c = \frac{D}{D_0} \sqrt{\frac{F^{ABS}}{F_0^{ABS}}} \quad (5.5)$$

$$\Delta c = \frac{c}{2} \left(\frac{\Delta F^{ABS}}{F^{ABS}} + \frac{\Delta F_0^{ABS}}{F_0^{ABS}} \right) \quad (5.6)$$

Finally, using Equation 5.5 and the data in Table 5.1 with $D_0 = 50$ cm as reference point, we can build Table 5.2. It is interesting to note that c for each value of D doesn't depend on the absorption factor.

Nominal ABS	Correction factor c		
	at $D = 155$ cm	at $D = 300$ cm	at $D = 400$ cm
1	$1.059 \pm 0.70\%$	$1.162 \pm 0.70\%$	$1.222 \pm 0.70\%$
2	$1.063 \pm 1.10\%$	$1.150 \pm 1.10\%$	$1.227 \pm 0.90\%$
5	$1.056 \pm 1.60\%$	$1.130 \pm 1.60\%$	$1.202 \pm 1.30\%$

Table 5.2: Correction factor c is computed thanks to formulae 5.5 taking as reference $D_0 = 50$ cm and the associated flux F_0^{ABS} for each absorption factor available in table 5.1.

678 For the range of D/D_0 values available, it is possible to use a simple linear fit to get the evolution
 679 of c . The linear fit will then use only 2 free parameters, a and b , as written in Equation 5.7. This gives
 680 us the results showed in Figure 5.13. Figure 5.13b confirms that using only a linear fit to extract c is
 681 enough as the evolution of the rate that can be obtained superimposes well on the simulation points.

$$c \left(\frac{D}{D_0} \right) = a \frac{D}{D_0} + b \quad (5.7)$$

$$F^{ABS} = F_0^{ABS} \left(a + \frac{bD_0}{D} \right)^2 \quad (5.8)$$

$$\Delta F^{ABS} = F^{ABS} \left[\frac{\Delta F_0^{ABS}}{F_0^{ABS}} + 2 \frac{\Delta a + \Delta b \frac{D_0}{D}}{a + \frac{bD_0}{D}} \right] \quad (5.9)$$

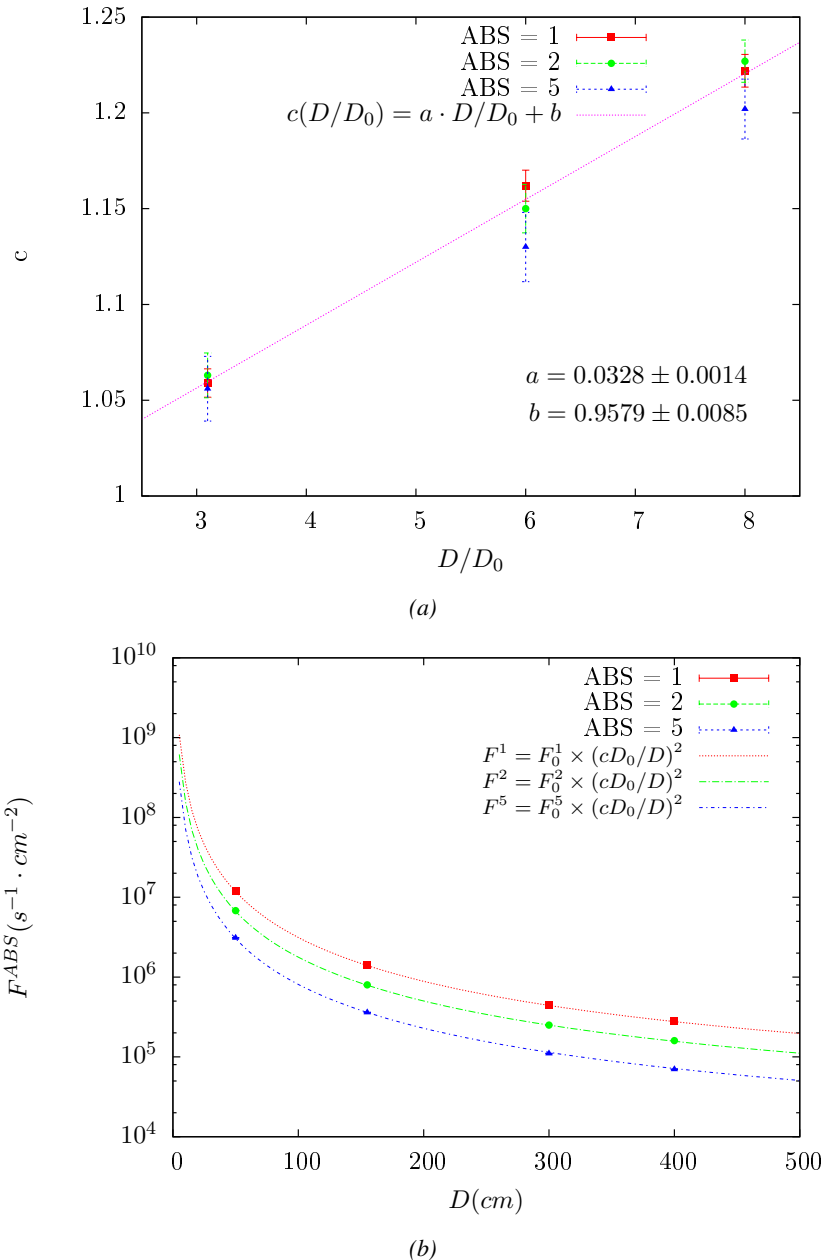


Figure 5.13: Figure 5.13a shows the linear approximation fit done via formulae 5.7 on data from table 5.2. Figure 5.13b shows a comparison of this model with the simulated flux using a and b given in figure 5.13a in formulae 5.4 and the reference value $D_0 = 50\text{cm}$ and the associated flux for each absorption factor F_0^{ABS} from table 5.1

In the case of the 2014 GIF tests, the RPC plane is located at a distance $D = 206\text{ cm}$ to the source. Moreover, to estimate the strength of the flux in 2014, it is necessary to consider the nuclear decay through time associated to the Cesium source whose half-life is well known ($t_{1/2} = (30.05 \pm 0.08)\text{ y}$). The very first source activity measurement has been done on the 5th of March 1997 while the GIF

686 tests where done in between the 20th and the 31st of August 2014, i.e. at a time $t = (17.47 \pm 0.02)$ y
 687 resulting in an attenuation of the activity from 740 GBq in 1997 to 494 GBq in 2014. All the needed
 688 information to extrapolate the flux through our detector in 2014 has now been assembled, leading
 689 to the Table 5.3. It is interesting to note that for a common RPC sensitivity to γ of $2 \cdot 10^{-3}$, the
 690 order of magnitude of the estimated hit rate per unit area is of the order of the kHz for the fully
 691 opened source. Moreover, taking profit of the two working absorbers, it will be possible to scan
 692 background rates at 0 Hz, ~ 300 Hz as well as ~ 600 Hz. Without source, a good estimate of the
 693 intrinsic performance will be available. Then at 300 Hz, the goal will be to show that the detectors
 694 fulfill the performance certification of CMS RPCs. Then a first idea of the performance of the
 695 detectors at higher background will be provided with absorption factors 2 (~ 600 Hz) and 1 (no
 696 absorption). *[Here I will also put a reference to the plot showing the estimated background rate at
 697 the level of RE3/1 in the case of HL-LHC but this one being in another chapter, I will do it later.]*

Nominal ABS	Photon flux F [$s^{-1}cm^{-2}$]			Hit rate/unit area [$Hz cm^{-2}$] at $D^{2014} = 206$ cm
	at $D_0^{1997} = 50$ cm	at $D_0^{1997} = 206$ cm	at $D^{2014} = 206$ cm	
1	$0.12 \cdot 10^8 \pm 0.2\%$	$0.84 \cdot 10^6 \pm 0.3\%$	$0.56 \cdot 10^6 \pm 0.3\%$	1129 ± 32
2	$0.68 \cdot 10^7 \pm 0.3\%$	$0.48 \cdot 10^6 \pm 0.3\%$	$0.32 \cdot 10^6 \pm 0.3\%$	640 ± 19
5	$0.31 \cdot 10^7 \pm 0.4\%$	$0.22 \cdot 10^6 \pm 0.3\%$	$0.15 \cdot 10^6 \pm 0.3\%$	292 ± 9

Table 5.3: The data at D_0 in 1997 is taken from [6]. In a second step, using Equations 5.8 and 5.9, the flux at D can be estimated in 1997. Then, taking into account the attenuation of the source activity, the flux at D can be estimated at the time of the tests in GIF in 2014. Finally, assuming a sensitivity of the RPC to γ $s = 2 \cdot 10^{-3}$, an estimation of the hit rate per unit area is obtained.

698 **5.2.4.2 Dose measurements**

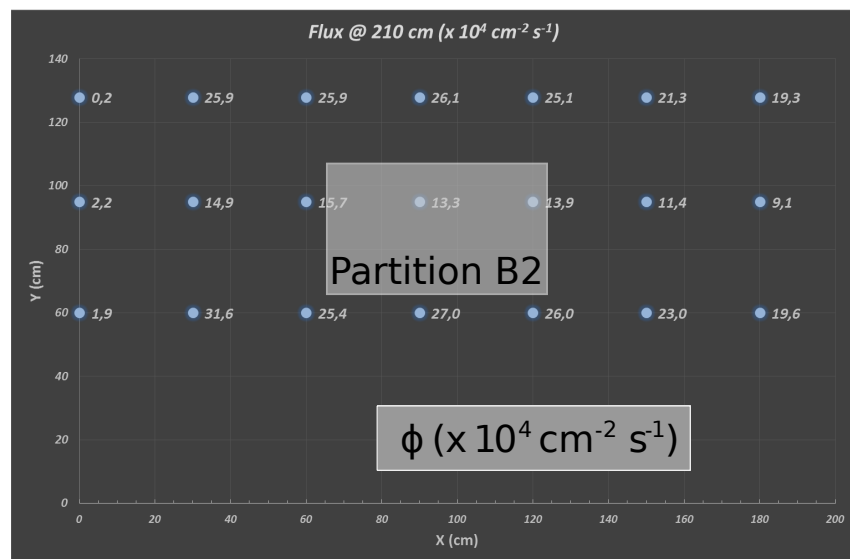


Figure 5.14: Dose measurements has been done in a plane corresponding to the tents front side. This plan is 1900 mm away from the source. As explained in the first chapter, a lens-shaped lead filter provides a uniform photon flux in the vertical plan orthogonal to the beam direction. If the second line of measured fluxes is not taken into account because of lower values due to experimental equipments in the way between the source and the tent, the uniformity of the flux is well showed by the results.

⁶⁹⁹ **5.2.5 Results and discussions**

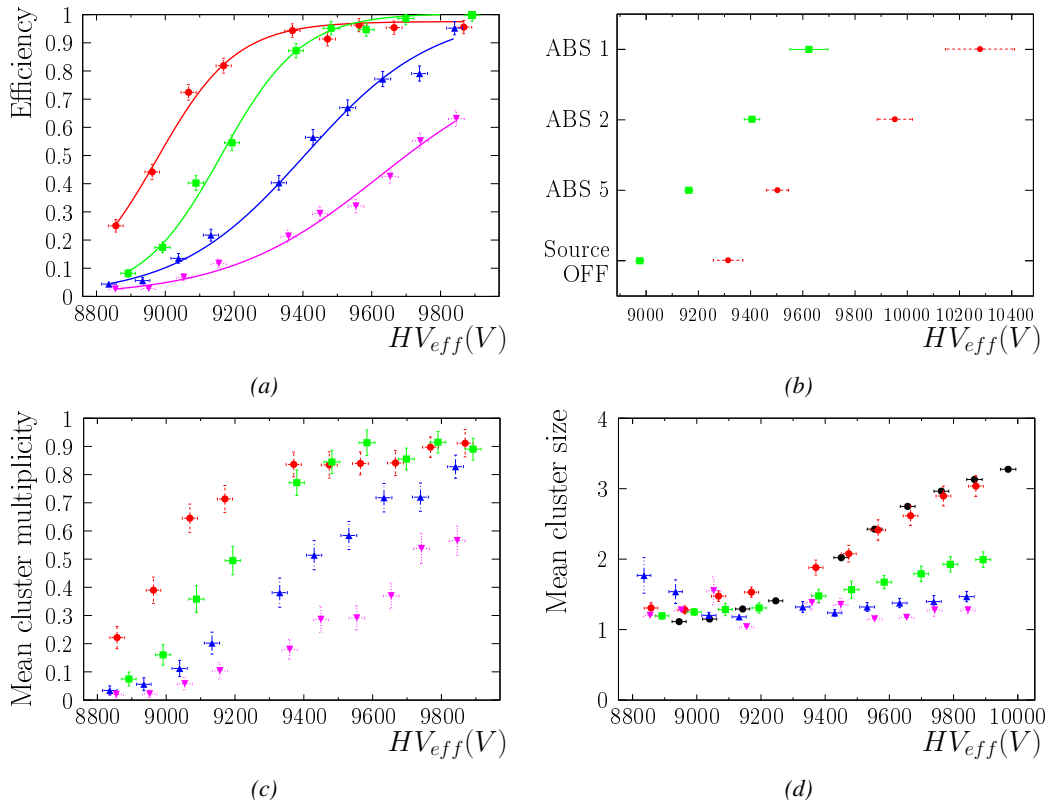


Figure 5.15

⁷⁰⁰ **5.3 Longevity tests at GIF++**

⁷⁰¹ Longevity studies imply a monitoring of the performance of the detectors probed using a high inten-
⁷⁰² sity muon beam in a irradiated environment by periodically measuring their rate capability, the dark
⁷⁰³ current running through them and the bulk resistivity of the Bakelite composing their electrodes.
⁷⁰⁴ GIF++, with its very intense ^{137}Cs source, provides the perfect environment to perform such kind
⁷⁰⁵ of tests. Assuming a maximum acceleration factor of 3, it is expected to accumulate the equivalent
⁷⁰⁶ charge in 1.7 years.

⁷⁰⁷ As the maximum background is found in the endcap, the choice naturally was made to focus the
⁷⁰⁸ GIF++ longevity studies on endcap chambers. Most of the RPC system was installed in 2007. Nev-
⁷⁰⁹ ertheless, the large chambers in the fourth endcap (RE4/2 and RE4/3) have been installed during
⁷¹⁰ LS1 in 2014. The Bakelite of these two different productions having different properties, four spare
⁷¹¹ chambers of the present system were selected, two RE2,3/2 spares and two RE4/2 spares. Having
⁷¹² two chambers of each type allows to always keep one of them non irradiated as reference, the per-
⁷¹³ formance evolution of the irradiated chamber being then compared through time to the performance
⁷¹⁴ of the non irradiated one.

⁷¹⁵ The performance of the detectors under different level of irradiation is measured periodically dur-
⁷¹⁶ ing dedicated test beam periods using the H4 muon beam. In between these test beam periods, the
⁷¹⁷ two RE2,3/2 and RE4/2 chambers selected for this study are irradiated by the ^{137}Cs source in order
⁷¹⁸ to accumulate charge and the gamma background is monitored, as well as the currents. The two
⁷¹⁹ remaining chambers are kept non-irradiated as reference detectors. Due to the limited gas flow in
⁷²⁰ GIF++, the RE4 chamber remained non-irradiated until end of November 2016 where a new mass
⁷²¹ flow controller has been installed allowing for bigger volumes of gas to flow in the system.

⁷²² Figures 5.16 and 5.17 give us for different test beam periods, and thus for increasing integrated
⁷²³ charge through time, a comparison of the maximum efficiency, obtained using a sigmoid-like func-
⁷²⁴ tion, and of the working point of both irradiated and non irradiated chambers [8]. No aging is yet to
⁷²⁵ see from this data, the shifts in γ rate per unit area in between irradiated and non irradiated detec-
⁷²⁶ tors and RE2 and RE4 types being easily explained by a difference of sensitivity due to the various
⁷²⁷ Bakelite resistivities of the HPL electrodes used for the electrode production.

⁷²⁸ Collecting performance data at each test beam period allows us to extrapolate the maximum effi-
⁷²⁹ ciency for a background hit rate of $300\text{ Hz}/\text{cm}^2$ corresponding to the expected HL-LHC conditions.
⁷³⁰ Aging effects could emerge from a loss of efficiency with increasing integrated charge over time,
⁷³¹ thus Figure 5.18 helps us understand such degradation of the performance of irradiated detectors in
⁷³² comparison with non irradiated ones. The final answer for an eventual loss of efficiency is given in
⁷³³ Figure 5.19 by comparing for both irradiated and non irradiated detectors the efficiency sigmoids
⁷³⁴ before and after the longevity study. Moreover, to complete the performance information, the Bake-
⁷³⁵ lite resistivity is regularly measured thanks to Ag scans (Figure 5.20) and the noise rate is monitored
⁷³⁶ weekly during irradiation periods (Figure 5.21). At the end of 2016, no signs of aging were observed
⁷³⁷ and further investigation is needed to get closer to the final integrated charge requirements proposed
⁷³⁸ for the longevity study of the present CMS RPC sub-system.

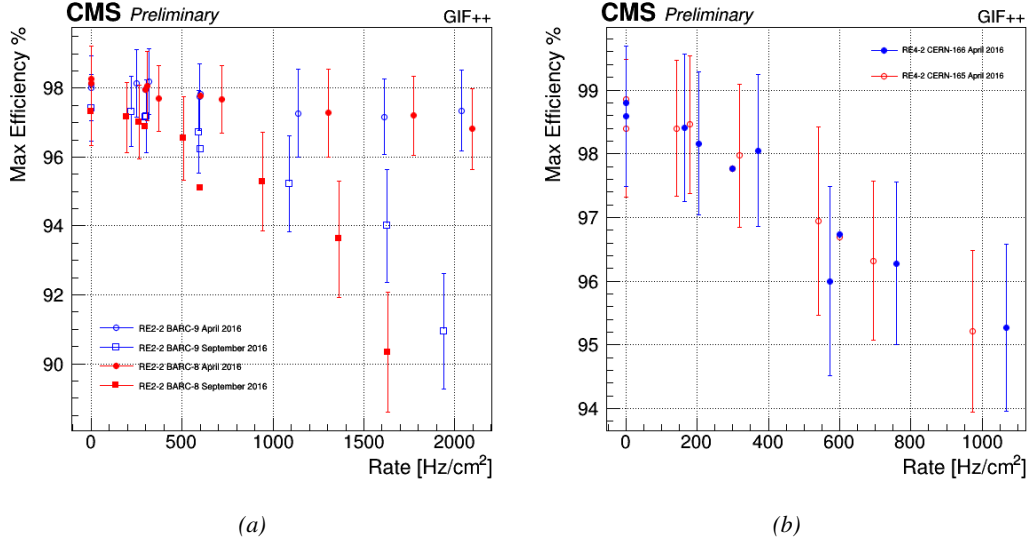


Figure 5.16: Evolution of the maximum efficiency for RE2 (5.16a) and RE4 (5.16b) chambers with increasing extrapolated γ rate per unit area at working point. Both irradiated (blue) and non irradiated (red) chambers are shown.

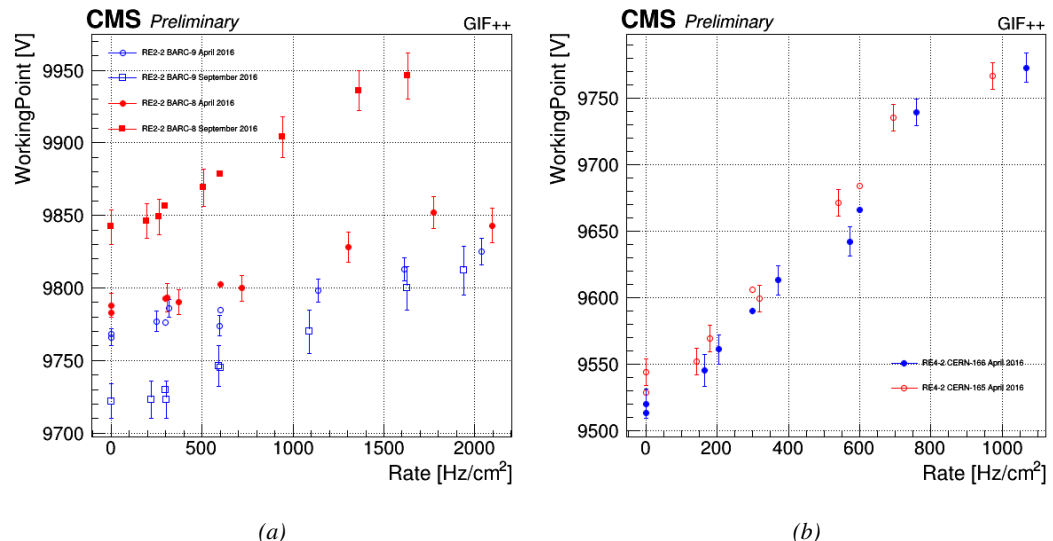


Figure 5.17: Evolution of the working point for RE2 (5.17a) and RE4 (5.17b) with increasing extrapolated γ rate per unit area at working point. Both irradiated (blue) and non irradiated (red) chambers are shown.

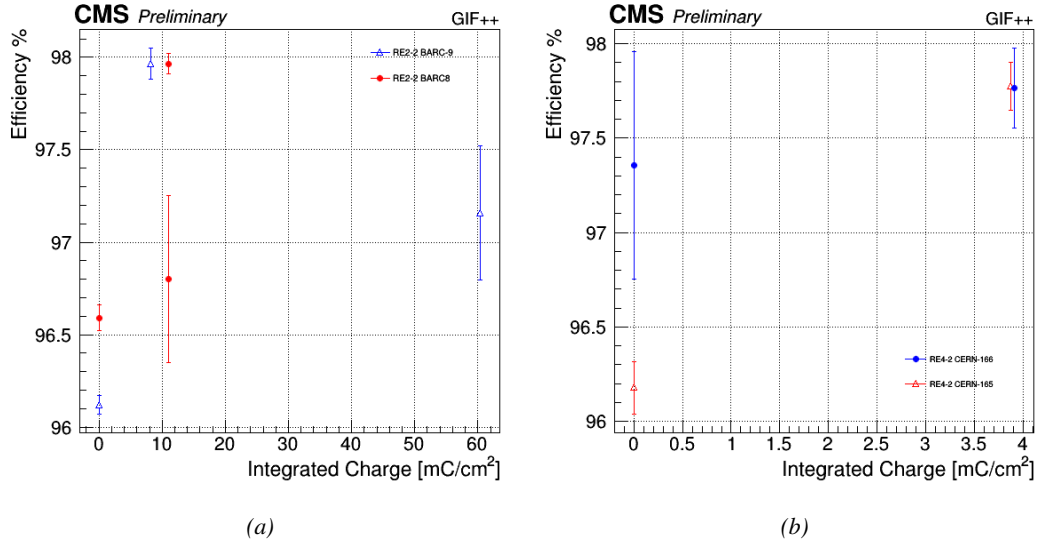


Figure 5.18: Evolution of the maximum efficiency at HL-LHC conditions, i.e. a background hit rate per unit area of $300 \text{ Hz}/\text{cm}^2$, with increasing integrated charge for RE2 (5.18a) and RE4 (5.18b) detectors. Both irradiated (blue) and non irradiated (red) chambers are shown. The integrated charge for non irradiated detectors is recorded during test beam periods and stays small with respect to the charge accumulated in irradiated chambers.

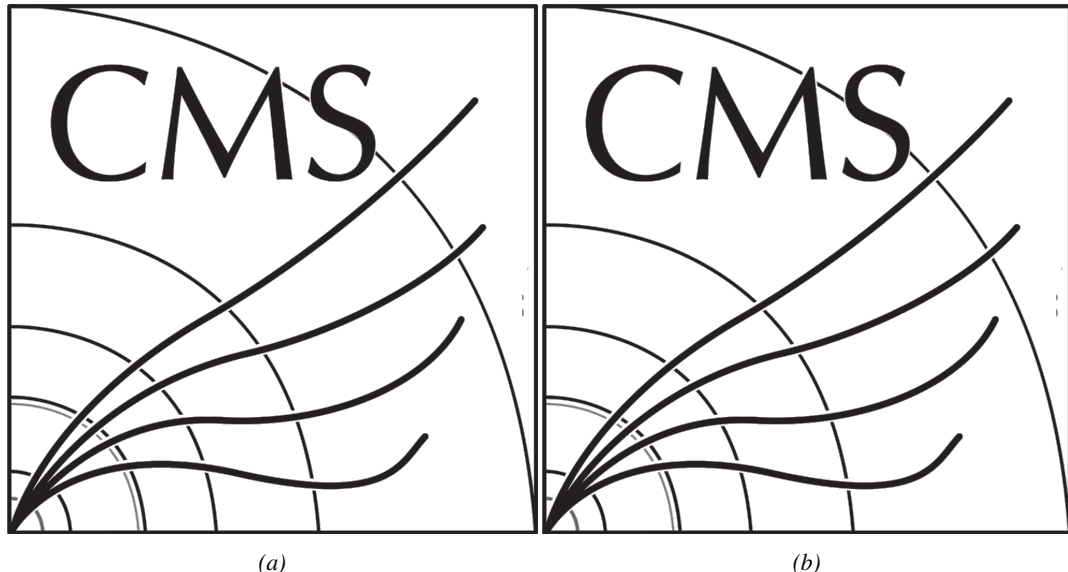


Figure 5.19: Comparison of the efficiency sigmoid before (triangles) and after (circles) irradiation for RE2 (5.19a) and RE4 (5.19b) detectors. Both irradiated (blue) and non irradiated (red) chambers are shown.

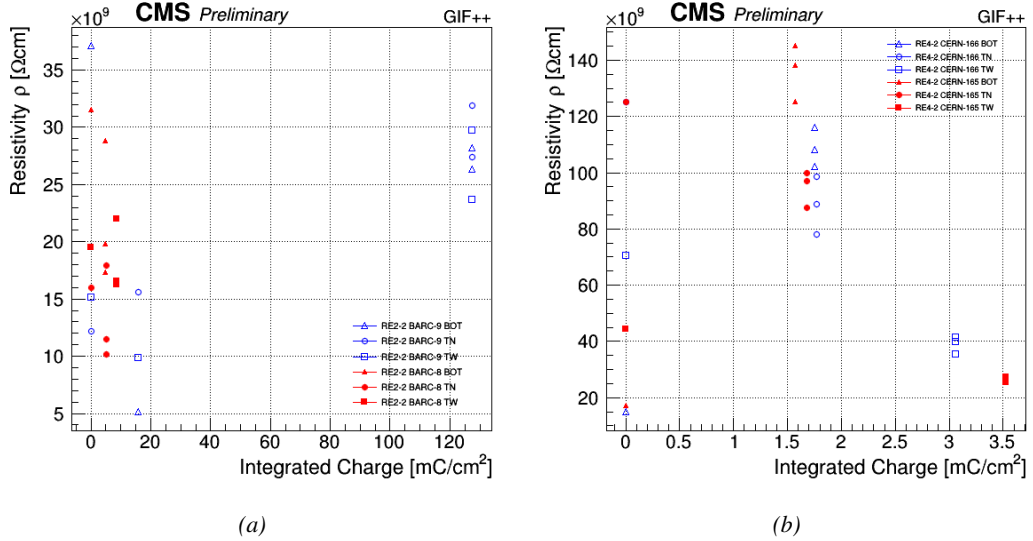


Figure 5.20: Evolution of the Bakelite resistivity for RE2 (5.20a) and RE4 (5.20b) detectors. Both irradiated (blue) and non-irradiated (red) chambers are shown.

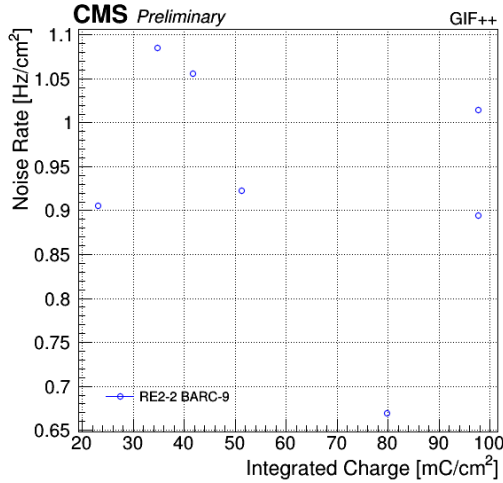


Figure 5.21: Evolution of the noise rate per unit area for the irradiated chamber RE2-2-BARC-9 only.

5.3.1 Description of the Data Acquisition

For the longevity studies, four spare chambers of the present system are used. Two spare RPCs of the RE2,3 stations as well as two spare RPCs from the new RE4 stations have been mounted in a Trolley. Six RE4 gaps are also placed in the trolley. The trolley is placed inside the GIFT++ in the upstream region of the bunker, taking the cesium source as a reference. The trolley is oriented for the detection surface of the chambers to be orthogonal to the beam line. The system can be moved along the orthogonal plane in order to have the beam in all η -partitions. For the aging the trolley is

747 moved outside the beam line and is placed in a distance of 5.2 m to the source, which irradiates the
 748 bunker using an attenuation filter of 2.2 which corresponds to a fluence of 10^7 gamma/cm^2 .

749 During GIF++ operation, the data collected can be divided into different categories as several
 750 parameters are monitored in addition to the usual RPC performance data. On one hand, to know
 751 the performance of a chamber, it is need to measure its efficiency and to know the background
 752 conditions in which it is operated. To do this, the hit signals from the chamber are recorded and
 753 stored in a ROOT file via a Data Acquisition (DAQ) software. On the other hand, it is also very
 754 important to monitor parameters such as environmental pressure and temperature, gas temperature
 755 and humidity, RPC HV, LV, and currents, or even source and beam status. This is done through the
 756 GIF++ web Detector Control Software (DCS) that stores this information in a database.

757 Two different types of tests are conducted on RPCs via the DAQ. Indeed, the performance of the
 758 detectors is measured periodically during dedicated test beam periods using the H4 muon beam. In
 759 between these test beam periods, when the beam is not available, the chambers are irradiated by the
 760 ^{137}Cs in order to accumulate deposited charge and the gamma background is measured.

761 RPCs under test are connected through LVDS cables to V1190A Time-to-Digital Converter
 762 (TDC) modules manufactured by CAEN. These modules, located in the rack area outside of the
 763 bunker, get the logic signals sent by the chambers and save them into their buffers. Due to the
 764 limited size of the buffers, the collected data is regularly erased and replaced. A trigger signal is
 765 needed for the TDC modules to send the useful data to the DAQ computer via a V1718 CAEN USB
 766 communication module.

767 In the case of performance test, the trigger signal used for data acquisition is generated by the
 768 coincidence of three scintillators. A first one is placed upstream outside of the bunker, a second one
 769 is placed downstream outside of the bunker, while a third one is placed in front of the trolley, close by
 770 the chambers. Every time a trigger is sent to the TDCs, i.e. every time a muon is detected, knowing
 771 the time delay in between the trigger and the RPC signals, signals located in the right time window
 772 are extracted from the buffers and saved for later analysis. Signals are taken in a time window of
 773 400 ns centered on the muon peak (here we could show a time spectrum). On the other hand, in the
 774 case of background rate measurement, the trigger signal needs to be "random" not to measure muons
 775 but to look at gamma background. A trigger pulse is continuously generated at a rate of 300 Hz using
 776 a dual timer. To integrate an as great as possible time, all signals contained within a time window of
 777 10us prior to the random trigger signal are extracted form the buffers and saved for further analysis
 778 (here another time spectrum to illustrate could be useful, maybe even place both spectrum together
 779 as a single Figure).

780 The signals sent to the TDCs correspond to hit collections in the RPCs. When a particle hits
 781 a RPC, it induce a signal in the pickup strips of the RPC readout. If this signal is higher than the
 782 detection threshold, a LVDS signal is sent to the TDCs. The data is then organised into 4 branches
 783 keeping track of the event number, the hit multiplicity for the whole setup, and the time and channel
 784 profile of the hits in the TDCs.

785 5.3.2 RPC current, environmental and operation parameter monitoring

786 In order to take into account the variation of pressure and temperature between different data taking
 787 periods the applied voltage is corrected following the relationship :

$$788 \text{HV}_{\text{eff}} = \text{HV}_{\text{app}} \times \left(0.2 + 0.8 \cdot \frac{P_0}{P} \times \frac{T}{T_0} \right) \quad (5.10)$$

788 where T_0 (=293 K) and P_0 (=990 mbar) are the reference values.

789 **5.3.3 Measurement procedure**

790 Insert a short description of the online tools (DAQ, DCS, DQM).

791 Insert a short description of the offline tools : tracking and efficiency algorithm.

792 Identify long term aging effects we are monitoring the rates per strip.

793 **5.3.4 Longevity studies results**

6

794

795

Investigation on high rate RPCs

796 **6.1 Rate limitations and ageing of RPCs**

797 **6.1.1 Low resistivity electrodes**

798 **6.1.2 Low noise front-end electronics**

799 **6.2 Construction of prototypes**

800 **6.3 Results and discussions**

7

801

802

Conclusions and outlooks

803 **7.1 Conclusions**

804 **7.2 Outlooks**

References

- [1] CERN. Geneva. LHC Experiments Committee. *The CMS muon project : Technical Design Report*. Tech. rep. CERN-LHCC-97-032. CMS Collaboration, 1997.
- [2] CERN. Geneva. LHC Experiments Committee. *Technical Proposal for the Phase-II Upgrade of the CMS Detector*. Tech. rep. CERN-LHCC-2015-010. CMS Collaboration, 2015.
- [3] CERN. Geneva. LHC Experiments Committee. *CMS, the Compact Muon Solenoid : technical proposal*. Tech. rep. CERN-LHCC-94-38. CMS Collaboration, 1994.
- [4] M. Abbrescia et al. “Study of long-term performance of CMS RPC under irradiation at the CERN GIF”. In: *NIMA* 533 (2004), pp. 102–106.
- [5] H.C. Kim et al. “Quantitative aging study with intense irradiation tests for the CMS forward RPCs”. In: *NIMA* 602 (2009), pp. 771–774.
- [6] S. Agosteo et al. “A facility for the test of large-area muon chambers at high rates”. In: *NIMA* 452 (2000), pp. 94–104.
- [7] PoS, ed. *CERN GIF ++ : A new irradiation facility to test large-area particle detectors for the high-luminosity LHC program*. Vol. TIPP2014. 2014, pp. 102–109.
- [8] M. Abbrescia et al. “Cosmic ray tests of double-gap resistive plate chambers for the CMS experiment”. In: *NIMA* 550 (2005), pp. 116–126.
- [9] A. Fagot. *GIF++ DAQ v4.0*. 2017. URL: https://github.com/afagot/GIF_DAQ.
- [10] CAEN. *Mod. V1190-VX1190 A/B, 128/64 Ch Multihit TDC*. 14th ed. 2016.
- [11] CAEN. *Mod. V1718 VME USB Bridge*. 9th ed. 2009.
- [12] W-Ie-Ne-R. *VME 6021-23 VXI*. 5th ed. 2016.
- [13] Wikipedia. *INI file*. 2017. URL: https://en.wikipedia.org/wiki/INI_file.
- [14] S. Carrillo A. Fagot. *GIF++ Offline Analysis v6*. 2017. URL: https://github.com/afagot/GIF_OfflineAnalysis.

A

829

830

831

A data acquisition software for CAEN VME TDCs

832 Certifying detectors in the perspective of HL-LHC required to develop tools for the GIF++ expe-
833 riment. Among them was the C++ Data Acquisition (DAQ) software that allows to make the com-
834 munications in between a computer and TDC modules in order to retrieve the RPC data [9]. In this
835 appendix, details about this software, as of how the software was written, how it functions and how
836 it can be exported to another similar setup, will be given.

837 A.1 GIF++ DAQ file tree

838 GIF++ DAQ source code is fully available on github at [https://github.com/afagot/GIF_](https://github.com/afagot/GIF_DAQ)
839 DAQ. The software requires 3 non-optional dependencies:

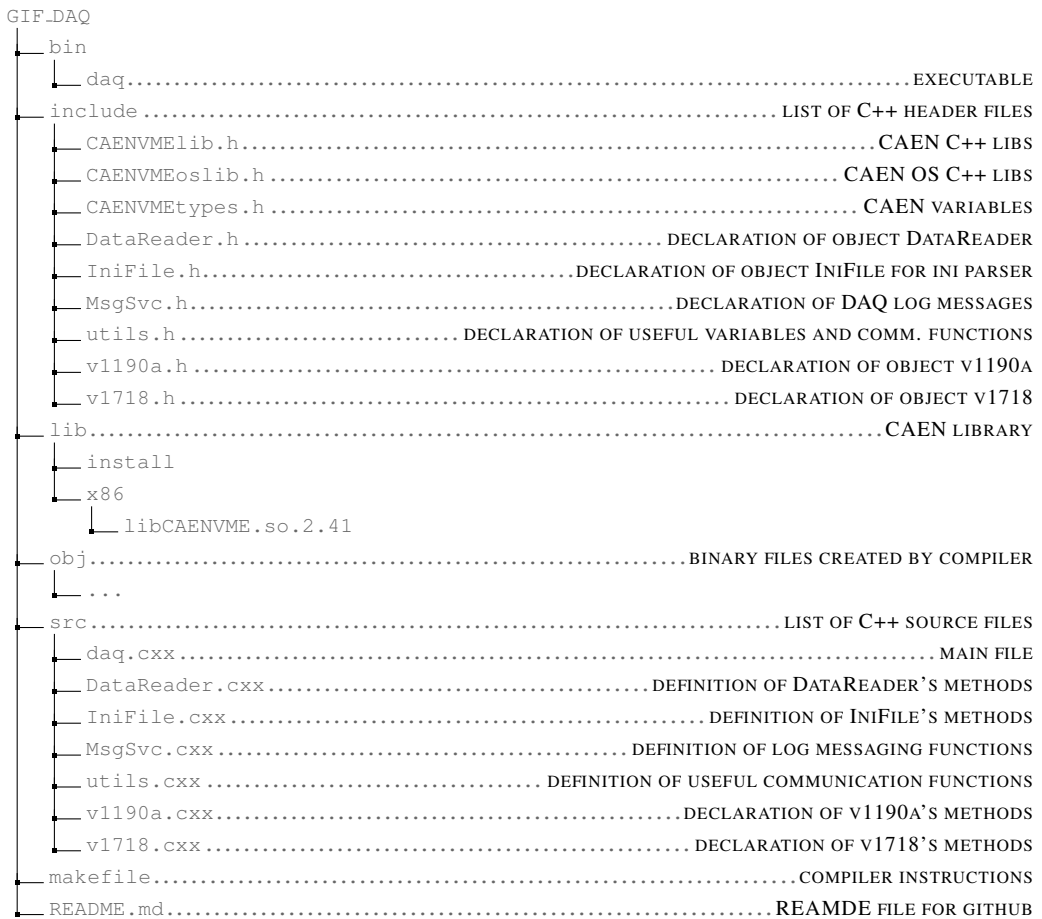
- 840 • CAEN USB Driver, to mount the VME hardware,
841 • CAEN VME Library, to communicate with the VME hardware, and
842 • ROOT, to organize the collected data into a TTree.

843 The CAEN VME library will not be packaged by distributions and will need to be installed man-
844 ually. To compile the GIF++ DAQ project via a terminal, from the DAQ folder use the command:

845
846 `make`

847 The source code tree is provided below along with comments to give an overview of the files' con-
848 tent. The different objects created for this project (`v1718`, `v1190a`, `IniFile` & `DataReader`) will be
849 described in details in the following sections.

850



851 A.2 Usage of the DAQ

852 GIF++ DAQ, as used in GIF++, is not a standalone software. Indeed, the system being more complex,
 853 the DAQ only is a sub-layer of the software architecture developed to control and monitor
 854 the RPCs that are placed into the bunker for performance study in an irradiated environment. The top
 855 layer of GIF++ is a Web Detector Control System (webDCS) application. The DAQ is only called
 856 by the webDCS when data needs to be acquired. The webDCS operates the DAQ through command
 857 line. To start the DAQ, the webDCS calls:

858
 859 bin/daq /path/to/the/log/file/in/the/output/data/folder

860 where /path/to/the/log/file/in/the/output/data/folder is the only argument required. This
 861 log file is important for the webDCS as this file contains all the content of the communication of the
 862 webDCS and the different systems monitored by the webDCS. Its content is constantly displayed
 863 during data taking for the users to be able to follow the operations. The communication messages
 864 are normally sent to the webDCS log file via the functions declared in file MsgSvc.h, typically
 865 MSG_INFO(string message).

866

A.3 Description of the readout setup

868 The CMS RPC setup at GIF++ counts 5 V1190A Time-to-Digital Converter (TDC) manufactured
 869 by CAEN [10]. V1190A are VME units accepting 128 independent Multi-Hit/Multi-Event TDC
 870 channels whose signals are treated by 4 100 ps high performance TDC chips developed by CERN
 871 / ECP-MIC Division. The communication between the computer and the TDCs to transfer data is
 872 done via a V1718 VME master module also manufactured by CAEN and operated from a USB
 873 port [11]. These VME modules are all hosted into a 6U VME 6021 powered crate manufactured by
 874 W-Ie-Ne-R than can accommodate up to 21 VME bus cards [12]. These 3 components of the DAQ
 875 setup are shown in Figure A.1.

876

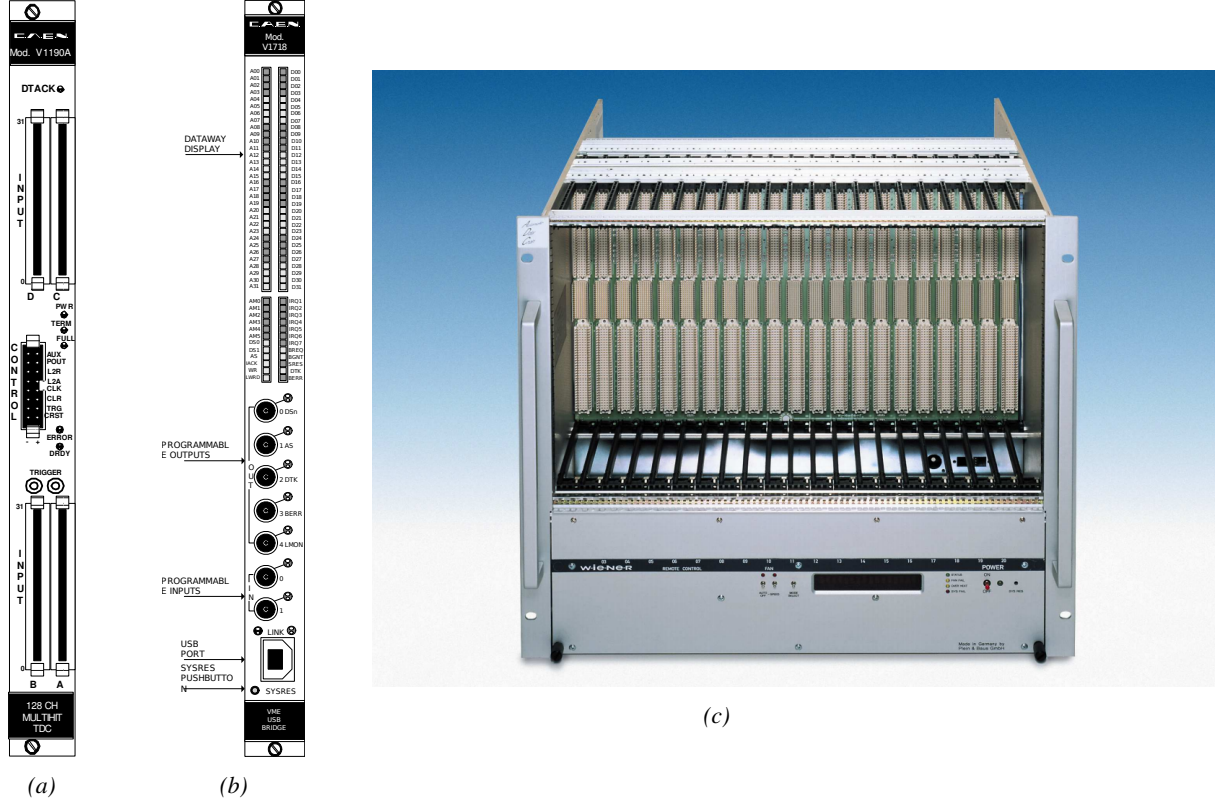


Figure A.1: (A.1a) View of the front panel of a V1190A TDC module [10]. (A.1b) View of the front panel of a V1718 Bridge module [11]. (A.1c) View of the front panel of a 6U 6021 VME crate [12].

877

A.4 Data read-out

878 To efficiently perform a data readout algorithm, C++ objects to handle the VME modules (TDCs
 879 and VME bridge) have been created along with objects to store data and read the configuration file

880 that comes as an input of the DAQ software.

881

882 A.4.1 V1190A TDCs

883 The DAQ used at GIF takes profit of the *Trigger Matching Mode* offered by V1190A modules.
 884 This setting is enabled through the method `v1190a::SetTrigMatching (int ntdcs)` where `ntdcs`
 885 is the total number of TDCs in the setup this setting needs to be enabled for (Source Code A.1). A
 886 trigger matching is performed in between a trigger time tag, a trigger signal sent into the TRIGGER
 887 input of the TDC visible on Figure A.1a, and the channel time measurements, signals recorded from
 888 the detectors under test in our case. Control over this data acquisition mode, explained through
 889 Figure A.2, is offered via 4 programmable parameters:

- 890 • **match window:** the matching between a trigger and a hit is done within a programmable time
 891 window. This is set via the method

```
892     void v1190a::SetTrigWindowWidth(UINT windowWidth, int ntdcs)
```

- 893 • **window offset:** temporal distance between the trigger tag and the start of the trigger matching
 894 window. This is set via the method

```
895     void v1190a::SetTrigWindowWidth(UINT windowWidth, int ntdcs)
```

- 896 • **extra search margin:** an extended time window is used to ensure that all matching hits are
 897 found. This is set via the method

```
898     void v1190a::SetTrigSearchMargin(UINT searchMargin, int ntdcs)
```

- 899 • **reject margin:** older hits are automatically rejected to prevent buffer overflows and to speed
 900 up the search time. This is set via the method

```
901     void v1190a::SetTrigRejectionMargin(UINT rejectMargin, int ntdcs)
```

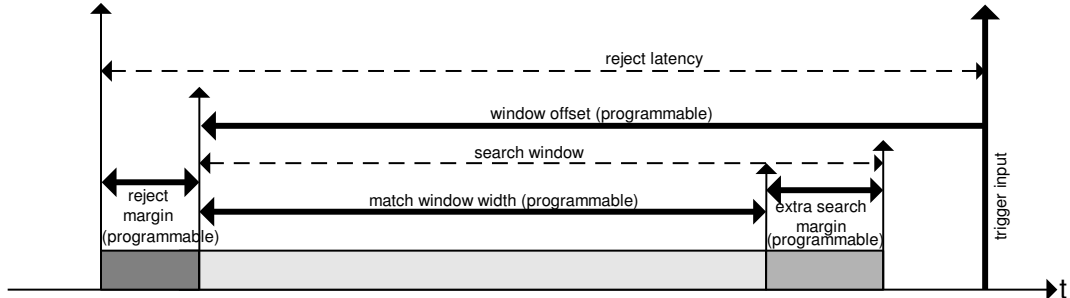


Figure A.2: Module V1190A Trigger Matching Mode timing diagram [10].

902 Each of these 4 parameters are given in number of clocks, 1 clock being 25 ns long. It is easy to
 903 understand at this level that there are 3 possible functioning settings:

- 904 • **1:** the match window is entirely contained after the trigger signal,

- 905 • **2:** the match window overlaps the trigger signal, or

- 906 • **3:** the match window is entirely contained before the trigger signal as displayed on Figure A.2.

907 In both the first and second cases, the sum of the window width and of the offset can be set to
908 a maximum of 40 clocks, which corresponds to 1 μ s. Evidently, the offset can be negative, allowing
909 for a longer match window, with the constraint of having the window ending at most 1 μ s after the
910 trigger signal. In the third case, the maximum negative offset allowed is of 2048 clocks (12 bit) cor-
911 responding to 51.2 μ s, the match window being strictly smaller than the offset. In the case of GIF++,
912 the choice has been made to use this last setting by delaying the trigger signal. During the studies
913 performed in GIF++, both the efficiency of the RPCs, probed using a muon beam, and the noise or
914 gamma background rate are monitored. The extra search and reject margins are left unused.
915 To probe the efficiency of RPC detectors, the trigger time tag is provided by the coïncidence of
916 scintillators when a bunch of muons passes through GIF++ area is used to trigger the data acquisi-
917 tion. For this measurement, it is useful to reduce the match window width only to contain the muon
918 information. Indeed, the delay in between a trigger signal and the detection of the corresponding
919 muon in the RPC being very contant (typically a few tens of ns due to jitter and cable length), the
920 muon signals are very localised in time. Thus, due to a delay of approximalety 325 ns in between
921 the muons and the trigger, the settings where chosen to have a window width of 24 clocks (600 ns)
922 centered on the muon peak thanks to a negative offset of 29 clocks (725 ns).
923 On the otherhand, monitoring the rates don't require for the DAQ to look at a specific time window.
924 It is important to integrate enough time to have a robust measurement of the rate as the number of
925 hits per time unit. The triggerring signal is provided by a pulse generator at a frequency of 300 Hz
926 to ensure that the data taking occurs in a random way, with respect to beam physics, to probe only
927 the irradiation spectrum on the detectors. The match window is set to 400 clocks (10 μ s) and the
928 negative offset to 401 clocks as it needs to exceed the value of the match window.

```

929
class v1190a
{
private :
    long             Handle;
    vector<Data32>   Address;
    CVDataWidth      DataWidth;
    CVAddressModifier AddressModifier;

public:

    v1190a(long handle, IniFile *inifile, int ntdcs);
    ~v1190a();
    Data16 write_op_req(Data32 address, int code, string error);
    Data16 read_op_req(Data32 address, string error);
    void Reset(int ntdcs);
    void Clear(int ntdcs);
    void TestWR(Data16 value,int ntdcs);
    void CheckTDCStatus(int ntdcs);
    void CheckCommunication(int ntdcs);
    void SetTDCTestMode(Data16 mode,int ntdcs);
    void SetTrigMatching(int ntdcs);
    void SetTrigTimeSubtraction(Data16 mode,int ntdcs);
    void SetTrigWindowWidth(Uint windowHeight,int ntdcs);
    void SetTrigWindowOffset(Uint windowOffset,int ntdcs);
    void SetTrigSearchMargin(Uint searchMargin,int ntdcs);
    void SetTrigRejectionMargin(Uint rejectMargin,int ntdcs);
    void GetTrigConfiguration(int ntdcs);
    void SetTrigConfiguration(IniFile *inifile,int ntdcs);
    void SetTDCDetectionMode(Data16 mode,int ntdcs);
    void SetTDCResolution(Data16 lsb,int ntdcs);
    void SetTDCDeadTime(Data16 time,int ntdcs);
    void SetTDCHeadTrailer(Data16 mode,int ntdcs);
    void SetTDCEventSize(Data16 size,int ntdcs);
    void SwitchChannels(IniFile *inifile,int ntdcs);
    void SetIRQ(Data32 level, Data32 count,int ntdcs);
    void SetBlockTransferMode(Data16 mode,int ntdcs);
    void Set(IniFile *inifile,int ntdcs);
    void CheckStatus(CVErrorCodes status) const;
    int ReadBlockD32(Uint tdc, const Data16 address,
                     Data32 *data, const Uint words, bool ignore_berr);
    Uint Read(RAWData *DataList,int ntdcs);
};

931

```

Source Code A.1: Description of C++ object v1190a.

The v1190a object, defined in the DAQ software as in Source Code A.1, offers the possibility to concatenate all TDCs in the readout setup into a single object containing a list of hardware addresses (addresses to access the TDCs' buffer through the VME crate) and each constructor and method acts on the list of TDCs.

936

937 A.4.2 DataReader

938 Enabled thanks to v1190a::SetBlockTransferMode(Data16 mode, int ntdcs), the data transfer
 939 is done via Block Transfer (BLT). Using BLT allows to tranfer a fixed number of events called a
 940 *block*. This is used together with an Almost Full Level (AFL) of the TDCs' output buffers, defined
 941 through v1190a::SetIRQ(Data32 level, Data32 count,int ntdcs). This AFL gives the maxi-

942 mum amount of 32735 words (16 bits, corresponding to the depth of a TDC output buffer) that can
943 written in a buffer before an Interrupt Request (IRQ) is generated and seen by the VME Bridge,
944 stopping the data acquisition to transfer the content of each TDC buffers before resuming. For each
945 trigger, 6 words or more are written into the TDC buffer:

- 946 • **a global header** providing information of the event number since the beginning of the data
947 acquisition,
- 948 • **a TDC header,**
- 949 • **the TDC data** (*if any*), 1 for each hit recorded during the event, providing the channel and the
950 time stamp associated to the hit,
- 951 • **a TDC error** providing error flags,
- 952 • **a TDC trailer,**
- 953 • **a global trigger time tag** that provides the absolute trigger time relatively to the last reset,
954 and
- 955 • **a global trailer** providing the total word count in the event.

956 As previously described in Section 4.4.3, CMS RPC FEEs provide us with 100 ns long LVDS
957 output signals that are injected into the TDCs' input. Any avalanche signal that gives a signal above
958 the FEEs threshold is thus recorded by the TDCs as a hit within the match window. Each hit is
959 assigned to a specific TDC channel with a time stamp, with a precision of 100 ps. The reference
960 time, $t_0 = 0$, is provided by the beginning of the match window. Thus for each trigger, coming from
961 a scintillator coïncidence or the pulse generator, a list of hits is stored into the TDCs' buffers and
962 will then be transferred into a ROOT Tree.

963 When the BLT is used, it is easy to understand that the maximum number of words that have
964 been set as AFL will not be a finite number of events or, at least, the number of events that would
965 be recorded into the TDC buffers will not be a multiple of the block size. In the last BLT cycle to
966 transfer data, the number of events to transfer will most probably be lower than the block size. In that
967 case, the TDC can add fillers at the end of the block but this option requires to send more data to the
968 computer and is thus a little slower. Another solution is to finish the transfer after the last event by
969 sending a bus error that states that the BLT reached the last event in the pile. This method has been
970 chosen in GIF++.

971 Due to irradiation, an event in GIF++ can count up to 300 words per TDC. A limit of 4096 words
972 (12 bits) has been set to generate IRQ which represent from 14 to almost 700 events depending on
973 the average of hits collected per event. Then the block size has been set to 100 events with enabled
974 bus errors. When an AFL is reached for one of the TDCs, the VME bridge stops the acquisition by
975 sending a BUSY signal.

976

979 The data is then transferred one TDC at a time into a structure called `RAWData` (Source Code A.2).

```
980
981     struct RAWData{
982         vector<int>           *EventList;
983         vector<int>           *NHitsList;
984         vector<int>           *QFlagList;
985         vector<vector<int>>   *ChannelList;
986         vector<vector<float>>  *TimeStampList;
987     };
```

982 *Source Code A.2: Description of data holding C++ structure `RAWData`.*

983 In order to organize the data transfer and the data storage, an object called `DataReader` was
984 created (Source Code A.3). On one hand, it has `v1718` and `v1190a` objects as private members for
985 communication purposes, such as VME modules settings via the configuration file `*iniFile` or data
986 read-out through `v1190a::Read()` and on the other hand, it contains the structure `RAWData` that allows
987 to organise the data in vectors reproducing the tree structure of a ROOT file.

```
988
989     class DataReader
990     {
991         private:
992             bool      StopFlag;
993             IniFile *iniFile;
994             Data32 MaxTriggers;
995             v1718 *VME;
996             int       nTDCs;
997             v1190a *TDCs;
998             RAWData TDCData;
999
1000         public:
1001             DataReader();
1002             virtual ~DataReader();
1003             void      SetIniFile(string inifilename);
1004             void      SetMaxTriggers();
1005             Data32 GetMaxTriggers();
1006             void      SetVME();
1007             void      SetTDC();
1008             int       GetQFlag(Uint it);
1009             void      Init(string inifilename);
1010             void      FlushBuffer();
1011             void      Update();
1012             string GetFileName();
1013             void      WriteRunRegistry(string filename);
1014             void      Run();
1015     };
```

990 *Source Code A.3: Description of C++ object `DataReader`.*

991 Each event is transferred from `TDCData` and saved into branches of a ROOT `TTree` as 3 integers
992 that represent the event ID (`EventCount`), the number of hits read from the TDCs (`nHits`), and the
993 quality flag that provides information for any problem in the data transfer (`qflag`), and 2 lists of
994 `nHits` elements containing the fired TDC channels (`TDCCh`) and their respective time stamps (`TDCTS`),
995 as presented in Source Code A.4. The ROOT file file is named using information contained into
996 the configuration file, presented in section A.5.2. The needed information is extracted using method
997 `DataReader::GetFileName()` and allow to build the output filename format `ScanXXXXXX_HVX_DAQ.root`

998 where ScanXXXXXX is a 6 digit number representing the scan number into GIF++ database and HVX
 999 the HV step within the scan that can be more than a single digit. An example of ROOT data file is
 1000 provided with Figure A.3.

```
1001
RAWData TDCData;
TFile *outputFile = new TFile(outputFileName.c_str(), "recreate");
TTree *RAWDataTree = new TTree("RAWData", "RAWData");

int EventCount = -9;
int nHits = -8;
int qflag = -7;
vector<int> TDCCh;
vector<float> TDCTS;

RAWDataTree->Branch("EventNumber", &EventCount, "EventNumber/I");
RAWDataTree->Branch("number_of_hits", &nHits, "number_of_hits/I");
RAWDataTree->Branch("Quality_flag", &qflag, "Quality_flag/I");
RAWDataTree->Branch("TDC_channel", &TDCCh);
RAWDataTree->Branch("TDC_TimeStamp", &TDCTS);

1002
//...
//Here read the TDC data using v1190a::Read() and place it into
//TDCData for as long as you didn't collect the requested amount
//of data.
//...

for(Uint i=0; i<TDCData.EventList->size(); i++){
    EventCount = TDCData.EventList->at(i);
    nHits = TDCData.NHitsList->at(i);
    qflag = TDCData.QFlagList->at(i);
    TDCCh = TDCData.ChannelList->at(i);
    TDCTS = TDCData.TimeStampList->at(i);
    RAWDataTree->Fill();
}
```

1003 *Source Code A.4: Highlight of the data transfer and organisation within DataReader::Run() after the data has been collected into TDCData.*

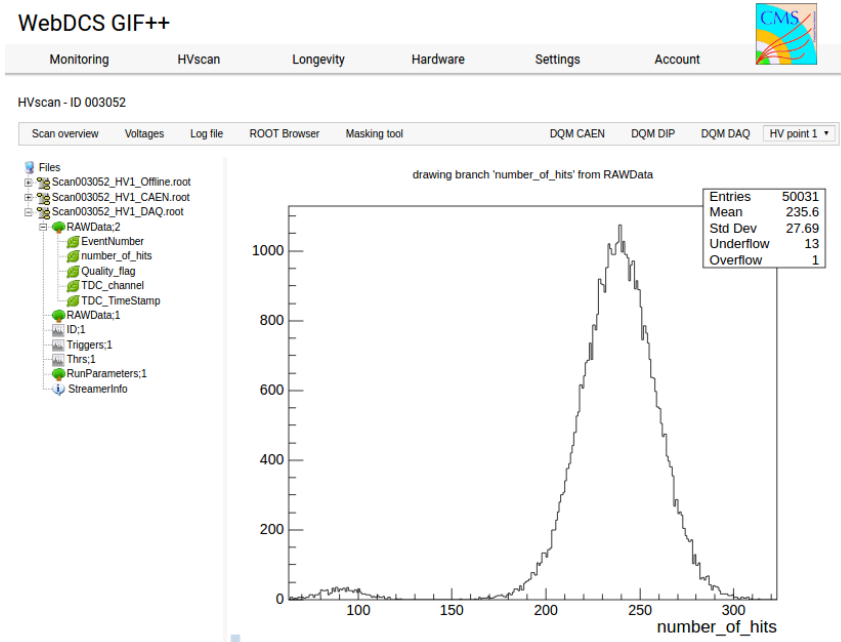


Figure A.3: Structure of the ROOT output file generated by the DAQ. The 5 branches (EventNumber, number_of_hits, Quality_flag, TDC_channel and TDC_TimeStamp) are visible on the left panel of the ROOT browser. On the right panel is visible the histogram corresponding to the variable nHits. In this specific example, there were approximately 50k events recorded to measure the gamma irradiation rate on the detectors. Each event is stored as a single entry in the TTree.

1004 A.5 Communications

1005 To ensure data readout and dialog in between the machine and the TDCs or in between the webDCS
 1006 and the DAQ, different communication solutions were used. First of all, it is important to have a
 1007 module to allow the communication in between the TDCs and the computer from which the DAQ
 1008 operates. When this communication is effective, shifters using the webDCS to control data taking
 1009 can thus send instructions to the DAQ.
 1010

1011 A.5.1 V1718 USB Bridge

1012 In the previous section, the data transfer as been discussed. The importance of the `v1718` object
 1013 (Source Code A.5), used as private member of `DataReader`, was not explicated. VME master
 1014 modules are used for communication purposes as they host the USB port that connects the pow-
 1015 ered crate buffer to the computer were the DAQ is installed. From the source code point of view,
 1016 this object is used to control the communication status, by reading the returned error codes with
 1017 `v1718::CheckStatus()`, or to check for IRQs coming from the TDCs through `v1718::CheckIRQ()`.
 1018 Finally, to ensure that triggers are blocked at the hardware level, a NIM pulse is sent out of one of the
 1019 5 programmable outputs (`v1718::SendBUSY()`) to the VETO of the coïndidence module where the
 1020 trigger signals originate from. As long as this signal is ON, no trigger can reach the TDCs anymore.

```

1021 class v1718{
1022     private:
1023         int Handle;
1024         Data32 Data;           // Data
1025         CVIRQLevels Level;    // Interrupt level
1026         CVAddressModifier AM; // Addressing Mode
1027         CVDataWidth dataSize; // Data Format
1028         Data32 BaseAddress;   // Base Address
1029
1030     public:
1031         v1718(IniFile *inifile);
1032         ~v1718();
1033         long GetHandle(void) const;
1034         int SetData(Data16 data);
1035         int GetData(void);
1036         int SetLevel(CVIRQLevels level);
1037         int GetLevel(void);
1038         int SetAM(CVAddressModifier am);
1039         int GetAM(void);
1040         int SetDatasize(CVDataWidth datasize);
1041         int GetDataSize(void);
1042         int SetBaseAddress(Data16 baseaddress);
1043         int GetBaseAddress(void);
1044         void CheckStatus(CVErrorCodes status) const;
1045         bool CheckIRQ();
1046         void SetPulsers();
1047         void SendBUSY(BusyLevel level);
1048     };

```

1023 *Source Code A.5: Description of C++ object v1718.*

1024 A.5.2 Configuration file

1025 The DAQ software takes as input a configuration file written using INI standard [13]. This file is
1026 partly filled with the information provided by the shifters when starting data acquisition using the
1027 webDCS, as shown by Figure A.4. This information is written in section [**General**] and will later
1028 be stored in the ROOT file that contains the DAQ data as can be seen from Figure A.3. Indeed,
1029 another **TTree** called **RunParameters** as well as the 2 histograms **ID**, containing the scan number,
1030 start and stop time stamps, and **Triggers**, containing the number of triggers requested by the shifter,
1031 are available in the data files. Moreover, **ScanID** and **HV** are then used to construct the file name
1032 thanks to the method **DataReader::GetFileName()**.

WebDCS GIF++

Monitoring HVscan Longevity Hardware Settings Account

DAQ High Voltage Scan

Type scan: Rate Scan Comments:

Source configuration: Source OFF U 333 D 333 HV after scan: Turn off

Beam configuration: Beam OFF

Waiting time: 1 (min)

Trigger mode: External Internal Random

Minimal measure time: 10 (min)

Chamber	RE2-2-NPD-BARC-8	RE2-2-CERN-105	RE2-2-NPD-BARC-9	RE4-2-CERN-105	RE4-2-KODEL-1-4	Max triggers
HV _{eff} 1	8600	8500	8600	8500	6500	<input type="text"/>
HV _{eff} 2	8700	8600	8700	8600	6600	<input type="text"/>
HV _{eff} 3	8800	8700	8800	8700	6700	<input type="text"/>
HV _{eff} 4	8900	8800	8900	8800	6800	<input type="text"/>
HV _{eff} 5	9000	8900	9000	8900	6900	<input type="text"/>
HV _{eff} 6	9100	9000	9100	9000	7000	<input type="text"/>
HV _{eff} 7	9200	9100	9200	9100	7100	<input type="text"/>
HV _{eff} 8	9300	9200	9300	9200	7200	<input type="text"/>
HV _{eff} 9	9400	9300	9400	9300	7300	<input type="text"/>
HV _{eff} 10	9500	9400	9500	9400	7400	<input type="text"/>

Start HV scan

Figure A.4: WebDCS DAQ scan page. On this page, shifters need to choose the type of scan (Rate, Efficiency or Noise Reference scan), the gamma source configuration at the moment of data taking, the beam configuration, and the trigger mode. These information will be stored in the DAQ ROOT output. Are also given the minimal measurement time and waiting time after ramping up of the detectors is over before starting the data acquisition. Then, the list of HV points to scan and the number of triggers for each run of the scan are given in the table underneath.

1033 The rest of the information is written beforehand in the configuration file template, as explicated
 1034 in Source Code A.6, and contains the hardware addresses to the different VME modules in the
 1035 setup as well as settings for the TDCs. As the TDC settings available in the configuration file are not
 1036 supposed to be modified, an improvement would be to remove them from the configuration file and
 1037 to hardcode them inside of the DAQ code itself or to place them into a different INI file that would
 1038 host only the TDC settings to lower the probability for a bad manipulation of the configuration file
 1039 that can be modified from one of webDCS' menus.

```

1040
[General]
Tdcs=4
ScanID=$scanid
HV=$HV
RunType=$runtype
MaxTriggers=$maxtriggers
Beam=$beam
[VMEInterface]
Type=V1718
BaseAddress=0xFF0000
Name=VmeInterface
[TDC0]
Type=V1190A
BaseAddress=0x00000000
Name=Tdc0
StatusA00-15=1
StatusA16-31=1
StatusB00-15=1
StatusB16-31=1
StatusC00-15=1
StatusC16-31=1
StatusD00-15=1
StatusD16-31=1
[TDC1]
Type=V1190A
BaseAddress=0x11110000
Name=Tdc1
StatusA00-15=1
StatusA16-31=1
StatusB00-15=1
StatusB16-31=1
StatusC00-15=1
StatusC16-31=1
StatusD00-15=1
StatusD16-31=1
1041
[TDC2]
Type=V1190A
BaseAddress=0x22220000
Name=Tdc2
StatusA00-15=1
StatusA16-31=1
StatusB00-15=1
StatusB16-31=1
StatusC00-15=1
StatusC16-31=1
StatusD00-15=1
StatusD16-31=1
[TDC3]
Type=V1190A
BaseAddress=0x44440000
Name=Tdc3
StatusA00-15=1
StatusA16-31=1
StatusB00-15=1
StatusB16-31=1
StatusC00-15=1
StatusC16-31=1
StatusD00-15=1
StatusD16-31=1
[TDCSettings]
TriggerExtraSearchMargin=0
TriggerRejectMargin=0
TriggerTimeSubstraction=0b1
TdcDetectionMode=0b01
TdcResolution=0b10
TdcDeadTime=0b00
TdcHeadTrailer=0b1
TdcEventSize=0b1001
TdcTestMode=0b0
BLTMode=1

```

Source Code A.6: INI configuration file template for 4 TDCs. In section [General], the number of TDCs is explicited and information about the ongoing run is given. Then, there are sections for each and every VME modules. There buffer addresses are given and for the TDCs, the list of channels to enable is given. Finally, in section [TDCSettings], a part of the TDC settings are given.

1043 A.5.3 WebDCS/DAQ intercommunication

1044 When shifters send instructions to the DAQ via the configuration file, it is the webDCS itself that
 1045 gives the start command to the DAQ and then the 2 softwares use inter-process communication
 1046 through file to synchronise themselves. This communication file is represented by the variable `const`
 1047 `string __runstatuspath`.

1048 On one side, the webDCS sends commands or status that are readout by the DAQ:

- 1049 • `INIT`, status sent when launching a scan and read via function `CtrlRunStatus(...)`,
- 1050 • `START`, command to start data taking and read via function `CheckSTART()`,
- 1051 • `STOP`, command to stop data taking at the end of the scan and read via function `CheckSTOP()`,
 1052 and
- 1053 • `KILL`, command to kill data taking sent by user and read via function `CheckKILL()`

1054 and on the other, the DAQ sends status that are controled by the webDCS:

- 1055 • `DAQ_RDY`, sent with `SendDAQReady()` to signify that the DAQ is ready to receive commands
 1056 from the webDCS,
- 1057 • `RUNNING`, sent with `SendDAQRunning()` to signify that the DAQ is taking data,
- 1058 • `DAQ_ERR`, sent with `SendDAQError()` to signify that the DAQ didn't receive the expected com-
 1059 mand from the webDCS or that the launch command didn't have the right number of argu-
 1060 ments,
- 1061 • `RD_ERR`, sent when the DAQ wasn't able to read the communication file, and
- 1062 • `WR_ERR`, sent when the DAQ wasn't able to write into the communication file.

1063 A.5.4 Example of inter-process communication cycle

1064 Under normal conditions, the webDCS and the DAQ processes exchange commands and status via
 1065 the file hosted at the address `__runstatuspath`, as explained in subsection A.5.3. An example of
 1066 cycle is given in Table A.1. In this example, the steps 3 to 5 are repeated as long as the webDCS tells
 1067 the DAQ to take data. A data taking cycle is the equivalent as what is called a *Scan* in GIFT++ jargon,
 1068 referring to a set a runs with several HV steps. Each repetition of steps 3 to 5 is then equivalent to a
 1069 single *Run*.

1070 At any moment during the data taking, for any reason, the shifter can decide that the data taking
 1071 needs to be stopped before it reached the end of the scheduled cycle. Thus at any moment on the
 1072 cycle, the content of the inter-process communication file will be changed to `KILL` and the DAQ will
 1073 shut down right away. The DAQ checks for `KILL` signals every 5s after the TDCs configuration is

step	actions of webDCS	status of DAQ	__runstatuspath
1	launch DAQ ramp voltages ramping over wait for currents stabilization	readout of IniFile configuration of TDCs	INIT
2		configuration done send DAQ ready wait for START signal	DAQ_RDY
3	waiting time over send START		START
4	wait for run to end monitor DAQ run status	data taking ongoing check for KILL signal	RUNNING
5		run over send DAQ_RDY wait for next DCS signal	DAQ_RDY
6	ramp voltages ramping over wait for currents stabilization		DAQ_RDY
3	waiting time over send START		START
4	wait for run to end monitor DAQ run status	update IniFile information data taking ongoing check for KILL signal	RUNNING
5		run over send DAQ_RDY wait for next DCS signal	DAQ_RDY
7	send command STOP	DAQ shuts down	STOP

Table A.1: Inter-process communication cycles in between the webDCS and the DAQ through file string signals.

1075 over. So far, the function `CheckKILL()` has been used only inside of the data taking loop of method
 1076 `DataReader::Run()` and thus, if the shifter decides to KILL the data taking during the TDC con-
 1077 figuration phase or the HV ramping in between 2 HV steps, the DAQ will not be stopped smoothly
 1078 and a *force kill* command will be sent to stop the DAQ process that is still awake on the computer.
 1079 Improvements can be brought on this part of the software to make sure that the DAQ can safely
 1080 shutdown at any moment.

1081

1082 A.6 Software export

1083 In section A.2 was discussed the fact that the DAQ as written in its last version is not a standalone
 1084 software. It is possible to make it a standalone program that could be adapted to any VME setup
 1085 using V1190A and V1718 modules by creating a GUI for the software or by printing the log mes-
 1086 sages that are normally printed in the webDCS through the log file, directly into the terminal. This
 1087 method was used by the DAQ up to version 3.0 moment where the webDCS was completed. Also, it
 1088 is possible to check branches of DAQ v2.X to have example of communication through a terminal.

1089

1090 DAQ v2.X is nonetheless limited in it's possibilities and requires a lot of offline manual interventions
1091 from the users. Indeed, there is no communication of the software with the detectors' power
1092 supply system that would allow for a user a predefine a list of voltages to operate the detectors at
1093 and loop over to take data without any further manual intervention. In v2.X, the data is taken for a
1094 single detector setting and at the end of each run, the softwares asks the user if he intends on taking
1095 more runs. If so, the software invites the user to set the operating voltages accordingly to what is
1096 necessary and to manual update the configuration file in consequence. This working mode can be a
1097 very first approach before an evolution and has been successfully used by colleagues from different
1098 collaborations.

1099

1100 For a more robust operation, it is recommended to develop a GUI or a web application to interface
1101 the DAQ. Moreover, to limit the amount of manual interventions, and thus the probability to
1102 make mistakes, it is also recommended to add an extra feature into the DAQ by installing the HV
1103 Wrapper library provided by CAEN of which an example of use in a similar DAQ software developped
1104 by a master student of UGent, and called TinyDAQ, is provided on UGent's github. Then, this
1105 HV Wrapper will help you communicating with and give instructions to a CAEN HV powered crate
1106 and can be added into the DAQ at the same level where the communication with the user was made
1107 in DAQ v2.X. In case you are using another kind of power system for your detectors, it is stringly
1108 adviced to use HV modules or crates that can be remotely controled via a using C++ libraries.

1109

B

1110

1111

Details on the offline analysis package

1112 The data collected in GIF++ thanks to the DAQ described in Appendix A is difficult to interpret by
1113 a human user that doesn't have a clear idea of the raw data architecture of the ROOT data files. In
1114 order to render the data human readable, a C++ offline analysis tool was designed to provide users
1115 with detector by detector histograms that give a clear overview of the parameters monitored during
1116 the data acquisition [14]. In this appendix, details about this software in the context of GIF++, as of
1117 how the software was written and how it functions will be given.

1118 B.1 GIF++ Offline Analysis file tree

1119 GIF++ Offline Analysis source code is fully available on github at https://github.com/aafagot/GIF_OfflineAnalysis. The software requires ROOT as non-optionnal dependency
1120 as it takes ROOT files in input and write an output ROOT file containing histograms. To compile the
1121 GIF++ Offline Analysis project is compiled with cmake. To compile, first a build/ directory must
1122 be created to compile from there:

```
1124 mkdir build  
1125 cd build  
1126 cmake ..  
1127 make  
1128 make install
```

1126 To clean the directory and create a new build directory, the bash script cleandir.sh can be used:

```
1127  
1128 ./cleandir.sh
```

1129 The source code tree is provided below along with comments to give an overview of the files' con-
1130 tent. The different objects created for this project (`Infrastructure`, `Trolley`, `RPC`, `Mapping`, `RPCHit`,
1131 `RPCCluster` and `Inifile`) will be described in details in the following sections.

1132

```

GIF_OfflineAnalysis
├── bin
│   └── offlineanalysis ..... EXECUTABLE
├── build..... CMAKE COMPILATION DIRECTORY
└── ...
    ├── include..... LIST OF C++ HEADER FILES
    │   ├── Cluster.h..... DECLARATION OF OBJECT RPCCLUSTER
    │   ├── Current.h..... DECLARATION OF GETCURRENT ANALYSIS MACRO
    │   ├── GIFTrolley.h..... DECLARATION OF OBJECT TROLLEY
    │   ├── Infrastructure.h..... DECLARATION OF OBJECT INFRASTRUCTURE
    │   ├── IniFile.h..... DECLARATION OF OBJECT INI FILE FORINI PARSER
    │   ├── Mapping.h..... DECLARATION OF OBJECT MAPPING
    │   ├── MsgSvc.h..... DECLARATION OF OFFLINE LOG MESSAGES
    │   ├── OfflineAnalysis.h..... DECLARATION OF DATA ANALYSIS MACRO
    │   ├── RPCTracker.h..... DECLARATION OF OBJECT RPC
    │   ├── RPCHit.h..... DECLARATION OF OBJECT RPCHIT
    │   ├── types.h..... DEFINITION OF USEFUL VARIABLE TYPES
    │   └── utils.h..... DECLARATION OF USEFUL FUNCTIONS
    ├── obj..... BINARY FILES CREATED BY COMPILER
    └── ...
        ├── src..... LIST OF C++ SOURCE FILES
        │   ├── Cluster.cc..... DEFINITION OF OBJECT RPCCLUSTER
        │   ├── Current.cc..... DEFINITION OF GETCURRENT ANALYSIS MACRO
        │   ├── GIFTrolley.cc..... DEFINITION OF OBJECT TROLLEY
        │   ├── Infrastructure.cc..... DEFINITION OF OBJECT INFRASTRUCTURE
        │   ├── IniFile.cc..... DEFINITION OF OBJECT INI FILE FORINI PARSER
        │   ├── main.cc..... MAIN FILE
        │   ├── Mapping.cc..... DEFINITION OF OBJECT MAPPING
        │   ├── MsgSvc.cc..... DEFINITION OF OFFLINE LOG MESSAGES
        │   ├── OfflineAnalysis.cc..... DEFINITION OF DATA ANALYSIS MACRO
        │   ├── RPCTracker.cc..... DEFINITION OF OBJECT RPC
        │   ├── RPCHit.cc..... DEFINITION OF OBJECT RPCHIT
        │   └── utils.cc..... DEFINITION OF USEFUL FUNCTIONS
        ├── cleandir.sh..... BASH SCRIPT TO CLEAN BUILD DIRECTORY
        ├── CMakeLists.txt..... SET OF INSTRUCTIONS FOR CMAKE
        ├── config.h.in..... DEFINITION OF VERSION NUMBER
        └── README.md..... README FILE FOR GITHUB

```

1133

B.2 Usage of the Offline Analysis

1134

In order to use the Offline Analysis tool, it is necessary to know the Scan number and the HV Step of the run that needs to be analysed. This information needs to be written in the following format:

1136

1137

```
Scan00XXXX_HVY
```

1138

where XXXX is the scan ID and Y is the high voltage step (in case of a high voltage scan, data will be taken for several HV steps). This format corresponds to the base name of data files in the database

1139

1140 of the GIF++ webDCS. Usually, the offline analysis tool is automatically called by the webDCS at
 1141 the end of data taking or by a user from the webDCS panel if an update of the tool was brought.
 1142 Nonetheless, an expert can locally launch the analysis for tests on the GIF++ computer, or a user can
 1143 get the code on its local machine from github and download data from the webDCS for its own anal-
 1144 ysis. To launch the code, the following command can be used from the `GIF_OfflineAnalysis` folder:

1145
 1146 `bin/offlineanalysis /path/to/Scan00XXXX_HVY`

1147 where, `/path/to/Scan00XXXX_HVY` refers to the local data files. Then, the offline tool will by itself
 1148 take care of finding all available ROOT data files present in the folder, as listed below:

- 1149
 - 1150 ● `Scan00XXXX_HVY_DAQ.root` containing the TDC data as described in Appendix ?? (events, hit
 and timestamp lists), and
 - 1151 ● `Scan00XXXX_HVY_CAEN.root` containing the CAEN mainframe data recorded by the monitor-
 ing tool webDCS during data taking (HVs and currents of every HV channels). This file is
 created independently of the DAQ.

1154 **B.2.1 Output of the offline tool**

1155 **B.2.1.1 ROOT file**

1156 The analysis gives in output ROOT datafiles that are saved into the data folder and called using the
 1157 naming convention `Scan00XXXX_HVY_Offline.root`. Inside those, a list of `TH1` histograms can be
 1158 found. Its size will vary as a function of the number of detectors in the setup as each set of histograms
 1159 is produced detector by detector. For each partition of each chamber, can be found:

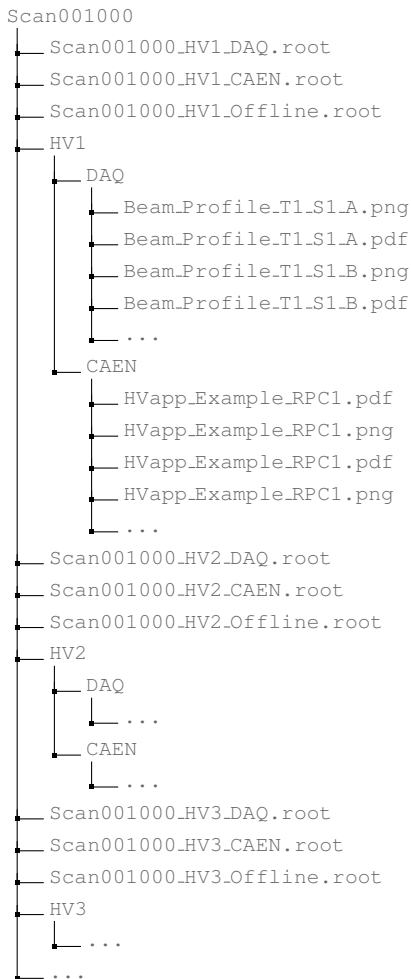
- 1160
 - 1161 ● `Time_Profile_Tt_Sc_p` shows the time profile of all recorded events (number of events per
 time bin),
 - 1162 ● `Hit_Profile_Tt_Sc_p` shows the hit profile of all recorded events (number of events per chan-
 nel),
 - 1164 ● `Hit_Multiplicity_Tt_Sc_p` shows the hit multiplicity (number of hits per event) of all recorded
 events (number of occurrences per multiplicity bin),
 - 1166 ● `Strip_Mean_Noise_Tt_Sc_p` shows noise/gamma rate per unit area for each strip in a se-
 lected time range. After filters are applied on `Time_Profile_Tt_Sc_p`, the filtered version
 of `Hit_Profile_Tt_Sc_p` is normalised to the total integrated time and active detection area
 of a single channel,
 - 1170 ● `Strip_Activity_Tt_Sc_p` shows noise/gamma activity for each strip (normalised version of
 previous histogram - strip activity = strip rate / average partition rate),
 - 1172 ● `Strip_Homogeneity_Tt_Sc_p` shows the *homogeneity* of a given partition ($\text{homogeneity} = \exp(-\text{strip rates standard deviation(strip rates in partition/average partition rate)})$),
 - 1174 ● `mask_Strip_Mean_Noise_Tt_Sc_p` shows noise/gamma rate per unit area for each masked
 strip in a selected time range. Offline, the user can control the noise/gamma rate and decide to
 mask the strips that are judged to be noisy or dead. This is done via the *Masking Tool* provided
 by the webDCS,

- 1178 ● `mask_Strip_Activity_Tt_Sc_p` shows noise/gamma activity per unit area for each masked
1179 strip with respect to the average rate of active strips,
- 1180 ● `NoiseCSize_H_Tt_Sc_p` shows noise/gamma cluster size, a cluster being constructed out of
1181 adjacent strips giving a signal at the *same time* (hits within a time window of 25 ns),
- 1182 ● `NoiseCMult_H_Tt_Sc_p` shows noise/gamma cluster multiplicity (number of reconstructed
1183 clusters per event),
- 1184 ● `Chip_Mean_Noise_Tt_Sc_p` shows the same information than `Strip_Mean_Noise_Tt_Scp` us-
1185 ing a different binning (1 chip corresponds to 8 strips),
- 1186 ● `Chip_Activity_Tt_Sc_p` shows the same information than `Strip_Activity_Tt_Scp` using
1187 chip binning,
- 1188 ● `Chip_Homogeneity_Tt_Sc_p` shows the homogeneity of a given partition using chip binning,
- 1189 ● `Beam_Profile_Tt_Sc_p` shows the estimated beam profile when taking efficiency scan. This
1190 is obtained by filtering `Time_Profile_Tt_Sc_p` to only consider the muon peak where the
1191 noise/gamma background has been subtracted. The resulting hit profile corresponds to the
1192 beam profile on the detector channels,
- 1193 ● `L0_Efficiency_Tt_Sc_p` shows the level 0 efficiency that was estimated **without** muon track-
1194 ing,
- 1195 ● `MuonCSize_H_Tt_Sc_p` shows the level 0 muon cluster size that was estimated **without** muon
1196 tracking, and
- 1197 ● `MuonCMult_H_Tt_Sc_p` shows the level 0 muon cluster multiplicity that was estimated **without**
1198 muon tracking.

1199 In the histogram labels, t stands for the trolley number (1 or 3), c for the chamber slot label in
1200 trolley t and p for the partition label (A, B, C or D depending on the chamber layout) as explained
1201 in Chapter 5.3.

1202 In the context of GIF++, an extra script called by the webDCS is called to extract the histograms
1203 from the ROOT files. The histograms are then stored in PNG and PDF formats into the correspond-
1204 ing folder (a single folder per HV step, so per ROOT file). the goal is to then display the histograms
1205 on the Data Quality Monitoring (DQM) page of the webDCS in order for the users to control the
1206 quality of the data taking at the end of data taking. An example of histogram organisation is given
1207 below:

1208
1209



1210 ***Here can put some screens from the webDCS to show the DQM and the plots available to users.***
 1211

1212 **B.2.1.2 CSV files**

1213 Moreover, up to 3 CSV files can be created depending on which ones of the 3 input files were in the
 1214 data folder:

- 1215 • **Offline-Rate.csv** : contains the summary of the noise/gamma hit and cluster rates for each
 1216 chamber partitions,
- 1217 • **Offline-Current.csv** : contains the summary of the currents and voltages applied on each
 1218 RPC HV channel, and
- 1219 • **Offline-L0-EffCl.csv** : contains the summary of the level 0 efficiency and muon cluster
 1220 information **without** tracking.

1221 Note that these 3 CSV files are created along with their *headers* (*offline-[...]-Header.csv*
 1222 containing the names of each data columns) and are automatically merged together when the offline

1223 analysis tool is called from the webDCS, contrary to the case where the tool is runned locally from
 1224 the terminal as the merging bash script is then not called. Thus, the resulting files, used to make
 1225 official plots, are:

```
1226     • Rate.csv ,  

1227     • Current.csv ,  

1228     • L0-EffCl.csv .
```

1229 **B.3 Analysis inputs and information handling**

1230 The usage of the Offline Analysis tool as well as its output have been presented in the previous sec-
 1231 tion. It is now important to dig further and start looking at the source code and the inputs necessary
 1232 for the tool to work. Indeed, appart from the raw ROOT data files that are analysed, more informa-
 1233 tion needs to be imported inside of the program to perform the analysis such as the description of
 1234 the setup inside of GIF++ at the time of data taking (number of trolleys, of RPCs, dimensions of the
 1235 detectors, etc...) or the mapping that links the TDC channels to the coresponding RPC channels in
 1236 order to translate the TDC information into human readable data. 2 files are used to transmit all this
 1237 information:

1238

- 1239 • Dimensions.ini, that provides the necessary setup and RPC information, and
- 1240 • ChannelsMapping.csv, that gives the link between the TDC and RPC channels as well as the
 1241 mask for each channel (masked or not?).

1242 **B.3.1 Dimensions file and IniFile parser**

1243 This input file, present in every data folder, allows the analysis tool to know of the number of ac-
 1244 tive trolleys, the number of active RPCs in those trolleys, and the details about each RPCs such as
 1245 the number of RPC gaps, the number of pseudo-rapidity partitions (for CMS-like prototypes), the
 1246 number of strips per partion or the dimensions. To do so, there are 3 types of groups in the INI file
 1247 architecture. A first general group, appearing only once at the head of the document, gives informa-
 1248 tion about the number of active trolleys as well as their IDs, as presented in Source Code B.1. For
 1249 each active trolley, a group similar to Source Code B.2 can be found containing information about
 1250 the number of active detectors in the trolley and their IDs. Finally, for each detector stored in slots
 1251 of an active trolley, there is a group providing information about their names and dimensions, as
 1252 showed in Source Code B.3.

```
1253 [General]  

1254 nTrolleys=2  

1255 TrolleysID=13
```

1255 *Source Code B.1: Example of **[General]** group as might be found in Dimensions.ini. In GIF++, only 2
 trolleys are available to hold RPCs and place them inside of the bunker for irradiation. The IDs of the trolleys
 are written in a signle string as "13" and then read character by character by the program.*

```
1256 [T1]
nSlots=4
SlotsID=1234
```

Source Code B.2: Example of trolley group as might be found in `Dimensions.ini`. In this example, the file tells that there are 4 detectors placed in the holding slots of the trolley T1 and that their IDs, written as a single string variable, are 1, 2, 3 and 4.

```
1257 [T1S1]
Name=RE2-2-NPD-BARC-8
Partitions=3
Gaps=3
Gap1=BOT
Gap2=TN
Gap3=TW
1258 AreaGap1=11694.25
AreaGap2=6432
AreaGap3=4582.82
Strips=32
ActiveArea-A=157.8
ActiveArea-B=121.69
ActiveArea-C=93.03
```

Source Code B.3: Example of slot group as might be found in `Dimensions.ini`. In this example, the file provides information about a detector named RE2-2-NPD-BARC-8, having 3 pseudo-rapidity readout partitions. This is a CMS RE2-2 type of detector. This information will then be used for example to compute the rate per unit area calculation.

This information is readout and stored in a C++ object called `IniFile`, that parses the information in the INI input file and stores it into a local buffer for later use. This INI parser is the exact same one that was previously developped for the GIF++ DAQ and described in Appendix A.5.2.

1263 B.3.2 TDC to RPC link file and Mapping

C

1264

1265

Structure of the hybrid simulation software

1266

C.1 Introduction

1267

insert text here...

